PETROGENESIS OF REE-MINERALIZED GRANITE DYKES IN THE NORTHEASTERN COBEQUID HIGHLANDS, NOVA SCOTIA

Shannon Broughm

Submitted in Partial Fulfillment of the Requirements

For the Degree of Bachelor of Sciences, Honours

Department of Earth Sciences

Dalhousie University, Halifax, Nova Scotia

Distribution License

DalSpace requires agreement to this non-exclusive distribution license before your item can appear on DalSpace.

NON-EXCLUSIVE DISTRIBUTION LICENSE

You (the author(s) or copyright owner) grant to Dalhousie University the non-exclusive right to reproduce and distribute your submission worldwide in any medium.

You agree that Dalhousie University may, without changing the content, reformat the submission for the purpose of preservation.

You also agree that Dalhousie University may keep more than one copy of this submission for purposes of security, back-up and preservation.

You agree that the submission is your original work, and that you have the right to grant the rights contained in this license. You also agree that your submission does not, to the best of your knowledge, infringe upon anyone's copyright.

If the submission contains material for which you do not hold copyright, you agree that you have obtained the unrestricted permission of the copyright owner to grant Dalhousie University the rights required by this license, and that such third-party owned material is clearly identified and acknowledged within the text or content of the submission.

If the submission is based upon work that has been sponsored or supported by an agency or organization other than Dalhousie University, you assert that you have fulfilled any right of review or other obligations required by such contract or agreement.

Dalhousie University will clearly identify your name(s) as the author(s) or owner(s) of the submission, and will not make any alteration to the content of the files that you have submitted.

If you have questions regarding this license please contact the repository manager at dalspace@dal.ca.

Grant the distribution license by signing and dating below.

_____ _____

Name of signatory Date

DALHOUSIE UNIVERSITY
Inspiring Minds

Department of Earth Sciences
Halifax, Nova Scotia
Canada B3H 4J1
(902) 494-2358
FAX (902) 494-6889

DATE: _____

AUTHOR: _____

TITLE: _____

_____

_____

_____

Degree: _____ Convocation: _____ Year: _____

Permission is herewith granted to Dalhousie University to circulate and to have copied for non-commercial purposes, at its discretion, the above title upon the request of individuals or institutions.

_____
Signature of Author

ABSTRACT

Granitoids enriched in incompatible elements have been the focus of ongoing exploration for rare earth elements around the world (REE's). High concentrations of REE's were discovered in 2010 at the contact zone between two Late Devonian to Early Carboniferous felsic igneous units in the Debert Lake area, northeastern Cobequid Highlands, Nova Scotia. Combined REE-concentrations range from 1800 to >7000 ppm within the REE-mineralized dykes. The main rock types present in the Debert Lake area include granitic rocks of the Hart Lake-Byers Lake (HLBL) pluton, felsic volcanic and volcaniclastic rocks of the Byers Brook Formation and late diorite bodies and diabase dykes. REE-mineralization is associated with a coarse-grained and pegmatitic arfvedsonite-bearing granitoid that is elevated in incompatible elements compared to the rest of the HLBL pluton. REE-mineralization occurs as late granitic dykes that cross cut all other rock types in the area and range from 1-50 cm wide. Less common are 1-25 cm wide segregated pods, within the arfvedsonite-bearing granitoid. In order to study the relationship between the HLBL pluton, the REE-enriched granitoids and the REE-mineralized dykes and pods, 19 samples were selected for petrographic study of differences in mineralogy and textures. Appropriate samples were analyzed using an electron-microprobe (EMP) for geochemical trends recorded by amphibole.

Petrographic studies show a change in amphibole composition based on color of pleochroism between each granitoid phase. Amphiboles within the incompatible-enriched granitoids consistently show dark-blue to black or greenish-brown to dark-blue pleochroism, indicative of arfvedsonite, compared to green to yellow pleochroism in the HLBL granite. This evidence is consistent with EMP results on amphiboles which show higher sodium and iron (arfvedsonite) content within the REE-enriched granitoids compared to the HLBL pluton, which have kataphorite amphibole. Harker variation plots of amphibole chemistry show discontinuous trends between the HLBL pluton and the REE-enriched/mineralized granite. Based on geochemical trends recored by the amphibole data, it is unlikely that the REE's were concentrated due solely to magma differentiation of the HLBL pluton.

Table of Contents

LIST OF FIGURES

LIST OF TABLES

ACKNOWLEDGMENTS

I am very appreciative of Shell for providing me with the funding to do all of the electron microprobe analysis and production of polished thin section. Thanks to Dan Macdonald for his help with any questions I had regarding the electron microprobe. Sincere thanks to honours coordinator Martin Gibling for his timely feedback and many comments on chapters throughout the year. I would like to thank my co-supervisor Trevor MacHattie for presenting me with the project and hiring me on as a summer student at NSDNR to do field work in my study area. Finally a thank-you to my supervisor Richard Cox for his expertise regarding my results, advice and feedback throughout the year.

CHAPTER 1: INTRODUCTION

1.1 Problem statement

In 2008 rare earth elements (REE) became the focus of exploration efforts around the world due to an increase in price to export these commodities from China, the largest producer of REE in the world (Canadian Chamber of Congress, 2012; Kerr and Rafuse, 2012). In 2010 rare earth element-mineralization was discovered in the northeastern Cobequid Highlands, in the Debert Lake area of Nova Scotia (MacHattie, 2011; Fig. 1.1). Alkaline to peralkaline igneous rocks are commonly characterized by enrichment in alkali metals, high-field strength elements (HFSE) and rare earth elements (REE), making them a target for exploration efforts (Schmitt et al., 2002; Boily and Williams-Jones, 1994). REE-mineralization in the Debert Lake area is concentrated in alkali-feldspar granite dykes that crosscut all other magmatic units in the area. The main magmatic rock types present include granitic rocks of the Hart Lake-Byers Lake (HLBL) pluton, felsic volcanic rocks of the Byers Brook Formation, and late diorite bodies and diabase dykes (MacHattie, 2011). REE-mineralization occurs in late granitic dykes that range from 1-50 cm wide and less commonly in 1-25 cm wide segregated pods (MacHattie, 2011). Total REE-concentrations in some of these dykes reach >7000ppm, which is approximately 20 times more concentrated than the HLBL granites (See Appendix A). REE minerals found in these dykes, listed with their key elements, include fergusonite (Nb), pyrochlore (Nb), chevkinite (Ce, La), allanite (Ce, La) and bastnaesite (Ce) (chemical formulas in table 1.1) (MacHattie, 2011)

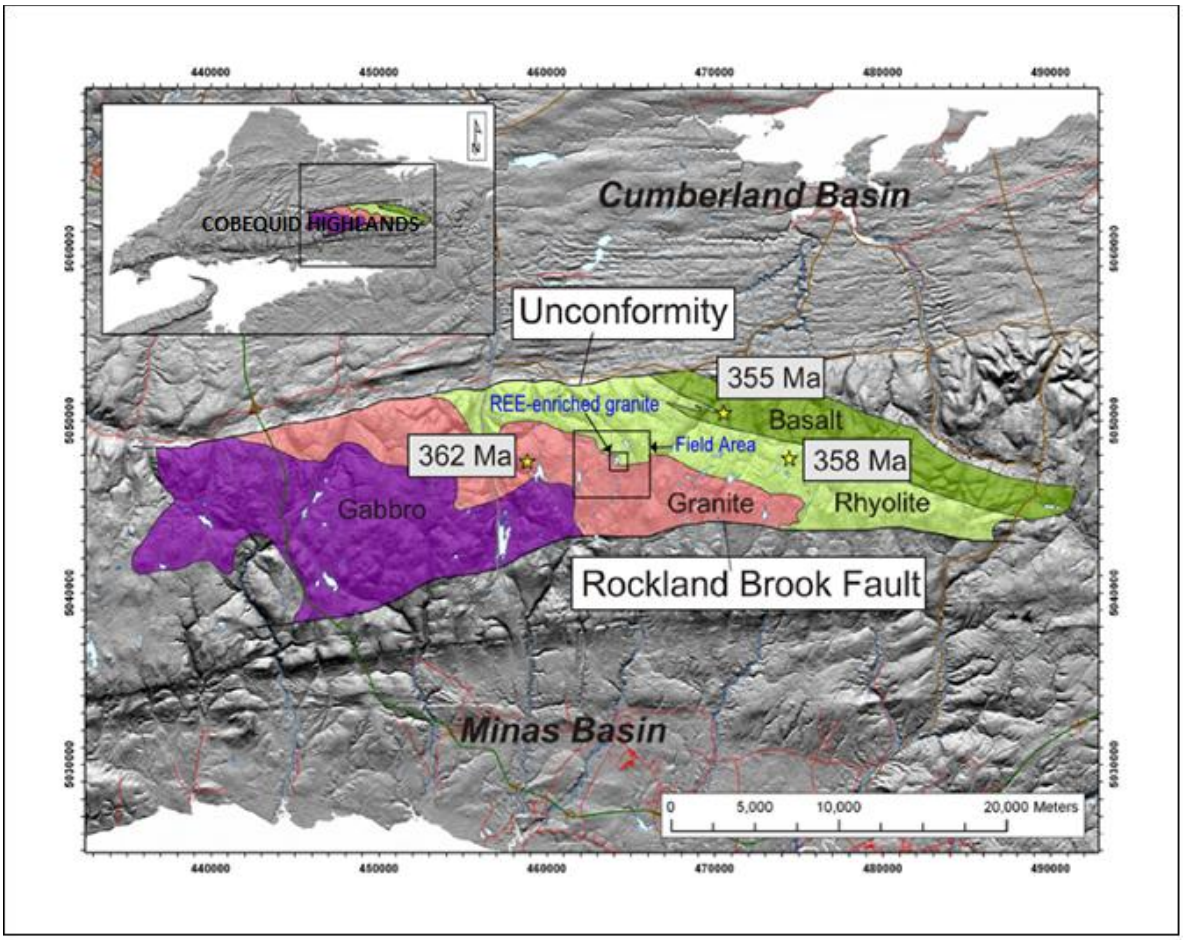

Figure 1.1: Geological map of the major Late Devonian to Early Carboniferous magmatic units of the eastern Cobequid Highlands. Stars show the approximate locations of U/Pb zircon crystallization ages (Doig et al. 1996); Dunning et al., 2002). Small square is the location of REE-enriched granite and larger square is the extent of the field area. Modified from (MacHattie, 2011)

The REE-mineralized dykes are believed to be associated with a coarse-grained and pegmatitic arfvedsonite-bearing alkali-feldspar granite that is elevated in incompatible elements (including REE's) compared to the rest of the HLBL pluton. This REE-enriched, arfvedsonite-bearing granitoid is located immediately south of the REE-mineralized dykes and southeast of Big Snare Lake (Fig. 4.1) and is also the host of REE-mineralized pods.

REE-mineral	Chemical Formula
Fergusonite	$YNbO_4$
Pyrochlore	$(Na, Ca)_2Nb_2O_6(OH,F)$
Chevkinite	$(Ce,La,Ca,Th)_4(Fe^{2+},Mg)_2(Ti,Fe^{3+})_3Si_4O_{22}$
Allanite	$(Ce,Ca,Y)_2(Al,Fe^{3+})_3(SiO_4)_3(OH)$
Bastnasite	$Ce(CO_3)F$

Table 1.1: Examples of the REE-minerals found in granite dykes in the Debert Lake area of Nova Scotia and their chemical formula.

The composition of amphibole in mildly peralkaline granites, such as the HLBL granites (Pe-Piper, 2002; Papoutsa, 2011), is known to reflect the bulk composition of the host rock (Mitchell, 1990). For this reason amphibole chemistry is useful for defining the magmatic evolution of the HLBL granites spatially associated with the REE-mineralized dykes and this will be the primary method used in this study.

1.2 Rare earth elements

1.2.1 What are rare earth elements?

Rare earth elements (REE) are a series of 17 elements, 15 of which are termed the lanthanides with atomic number 57-71 on the periodic table of elements, plus yttrium and scandium due to their similar physical and chemical properties. REE's are rather abundant in the earth's crust despite their name; some REE's are equally or more abundant than other economically important metals including copper, lead, nickel and zinc (Davies, 2010). Gold is 200 times less abundant than the least abundant naturally occurring REE (Davies, 2010). REE's have an overall crustal abundance that ranges from 150 to 220 parts per million (ppm) (Long, 2010). Economically viable REE deposits result from concentration of REE metals, commonly due to a combination of magmatic and hydrothermal processes in alkaline to peralkaline igneous bodies (Boily and Williams-Jones, 1994; Salvi and Williams-Jones, 1996)

Rare Earth Element	Estimate of crustal abundance (Lide, 1997)	Primitive mantle normalization (Sun & McDonough, 1989)
La	39	0.687
Ce	66.5	1.775
Pr	9.2	0.276
Nd	41.5	1.354
Sm	7.05	0.444
Eu	2	0.168
Gd	6.2	0.596
Tb	1.2	0.108
Dy	5.2	0.737
Ho	1.3	0.164
Er	3.5	0.48
Tm	0.52	0.068
Yb	0.52	0.493
Lu	3.2	0.074

Table 1.2: Estimates of rare earth element abundances within the crust and primitive mantle.

1.2.2 Importance of rare earth elements to modern society

REE's are essential components in a wide range of advanced technologies and electronic applications such as cell phones, laptops and televisions (Davies, 2010). They are necessary constituents in catalysts used for petroleum fluid cracking and automotive pollution control converters. REE's are used in renewable energy technologies like hybrid cars and wind power generators, an industry that is rapidly growing (Davies, 2010). REE's are also essential components in defense applications needed for national security such as missiles, lasers, satellite communications and jet engines (Davies, 2010). With technologies continuously advancing and becoming more available to the general public, a continuous increase in demand for REE's is expected.

1.2.3 Importance of rare earth element exploration

China currently controls 97 percent the world's production of REE's (U.S Congressional Research Service, 2012). Since 2008, China has implemented a number of restrictions on the export of REE's (Kerr and Rafuse, 2012). With interests in REE's and their applications growing globally, it has become increasingly important to find REE deposits outside China. In 2011, the Mountain Pass mine in California restarted production of REE's and is continuing to expand production (Canadian Chamber of Congress, 2012). A number of REE deposits are being explored for future development in Canada, including the Nechalacho REE deposit in Northwest Territories and Strange Lake deposit in Quebec (Canadian Chamber of Congress, 2012).

1.3 Scope of the study

This study was initiated to help understand the origin of REE-mineralized granite dykes in the Debert Lake area of Nova Scotia. The REE-mineralized granite represents the latest magmatic event in the area as shown by crosscutting relationships (Fig. 3.1). Concentration of REE's may be facilitated by fractional crystallization within a magma chamber (Kerr, 2012). To study whether fractional crystallization played a role in concentrating the REE's from the HLBL pluton to the REE-enriched granitoids and finally the REE-mineralized dykes, 19 samples were selected for petrographic study to identify differences in mineralogy and texture. Selected samples were analyzed using an electron-microprobe (EMP) to examine the geochemical trends recorded by the amphiboles present. Amphiboles are a useful mineral to study geochemically because they have a broad chemical composition that can be related to the bulk composition of their host rock (Mitchell, 1990). With both geochemistry and petrography we hope to better define how REE's concentrated within the REE-mineralized dykes.

CHAPTER 2: REGIONAL GEOLOGICAL FRAMEWORK

2.1 Tectonic setting of the Cobequid Highlands

The Cobequid Highlands are located just north of the boundary between the Avalon and Meguma terranes at the northern extension of the Appalachian orogenic belt (Fig 2.1)(Calder, 1998, Pe-Piper and Piper, 2002). The Cobequid-Chedabucto fault zone marks the crustal-scale boundary between the two terranes, located at the southern margin of the Cobequid Highlands (fig 2.1). This fault zone consists of a series of dominantly dextral strike-slip faults with various stages of displacement and a wide range of ages (Pe-Piper and Piper, 2002) and is the upper crustal expression of the Minas Geofracture (Keppie, 1987). The Minas Geofracture separates the Meguma from the Avalon terrane (Donohoe and Wallace 1982; Williams, 1982). The accretion of the Meguma and Avalon terranes onto Laurentia by the Silurian was one of the many major tectono-thermal events of the Acadian Orogeny, building the Appalachian Mountain chain across the east coast of North America (Hicks et al. 1999). Regional extension followed the Acadian Orogeny, resulting in opening of the Magdalen Basin and re-activation of the Neoproterozoic Rockland Brook Fault during the late Paleozoic (Pe-Piper and Piper, 2002). Re-activation was associated with thrusting and wall-rock compression as well as lateral translation of blocks on either side of the Rockland Brook Fault. This movement allowed for the emplacement of Late Devonian to Early Carboniferous igneous units along the Rockland Brook Fault (Fig. 2.1) (Pe-Piper and Piper, 2002). The Rockland Brook Fault is a splay of the Cobequid- Chedabucto fault and is the

main fault of the eastern Cobequid Highlands, most active during the Late Paleozoic (Koukouvelas et al., 2006).

2.2 Igneous units of the northeastern Cobequid Highlands

2.2.1 General geology

The Wentworth Plutonic Complex is located in the eastern Cobequid Highlands, just north of the Rockland Brook Fault (Fig. 1.1). The plutonic complex comprises four major magmatic units. From west to east these units include gabbro of the Folly Lake Pluton, granitic rocks of the HLBL Pluton, rhyolite of the Byers Brook Formation and basalt of the Diamond Brook Formation (Fig 1.1) (Pe-Piper, 1998; MacHattie, 2011). Pe-Piper and Piper (2002) introduced the term Wentworth Pluton to group together the Folly Lake Pluton and the HLBL Pluton, earlier defined by Donohoe and Wallace (1982). This was mainly due to the difficulty identifying the two units in the field (Papoutsa, 2011). Bimodal magmatism of mafic/intermediate rocks and granitic rocks show both intermingling and crosscutting relationships across extensive areas of both plutons (Papoutsa, 2011; MacHattie, 2011; Pe-Piper, 2002). For the purpose of this thesis I will continue to use the nomenclature introduced by Donohoe and Wallace (1982) because my field samples only include granitic rocks of the HLBL pluton.

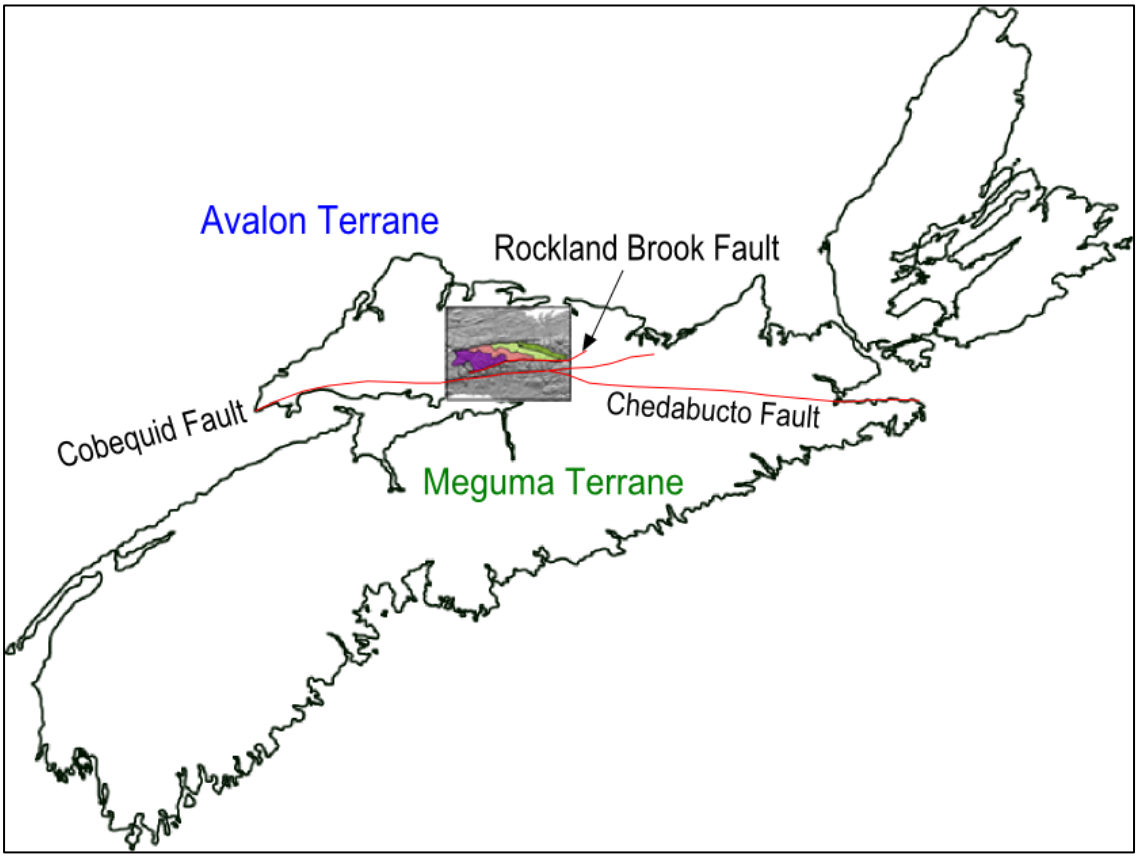

Figure 1. 1: Location of the Cobequid-Chedabucto fault zone across central Nova Scotia marking the boundary between the Meguma and Avalon Terranes. The Rockland Brook Faults, a splay of the Cobequid fault, facilitated the emplacement of Late Devonian to Early Carboniferous igneous units (shown in purple, pink and shades of green on map) of the eastern Cobequid Highlands.

2.2.2 Geochronology of igneous units

U/Pb zircon crystallization ages of the major magmatic units in the northeastern Cobequid Highlands suggest that magmatism occurred during latest Devonian to earliest Carboniferous (Fig 2.2). Granite of the HLBL pluton recorded a U/Pb zircon age of 362 ± 2 Ma (Doig et al., 1996) and an Ar-Ar (sodic-amphibole) age of 358 ± 4Ma (Pe-Piper et al., 2004). Rhyolite of the Byers Brook formation recorded a zircon age of 358 ± 1 Ma and the Diamond Brook Formation yielded a zircon age of 355 ± 3 Ma (Dunning et al., 2002). The Folly Lake gabbro yielded ages of 357 ± 2Ma and 353 ± 2Ma, from Ar-Ar hornblende and Ar-Ar biotite, respectively (Pe-Piper et al., 2004)

Based on the above age dating studies, the geological evolution of the major magmatic units in the northeastern Cobequid Highlands can be divided into three main events. The first event involved the emplacement of granitic rocks of the HLBL Pluton at depth and the extrusion of felsic volcanic-volcaniclastic rocks of the Byers Brook Formation at the surface between 364-357 Ma (MacHattie, 2011). The second event involved the intrusion of gabbro/diorite of the Folly Lake Pluton into the base of the HLBL Pluton and emplacement of its extrusive equivalent, basalt lava flows of the Diamond Brook Formation between 357-351 Ma. This event included the cogenetic emplacement of diabase dykes and diorite within the HLBL Pluton (MacHattie, 2011). The third event between 351-310 Ma involved the tectonic exhumation of each of these units into their current sub-vertical, northwest-southeast trending orientation (MacHattie, 2011).

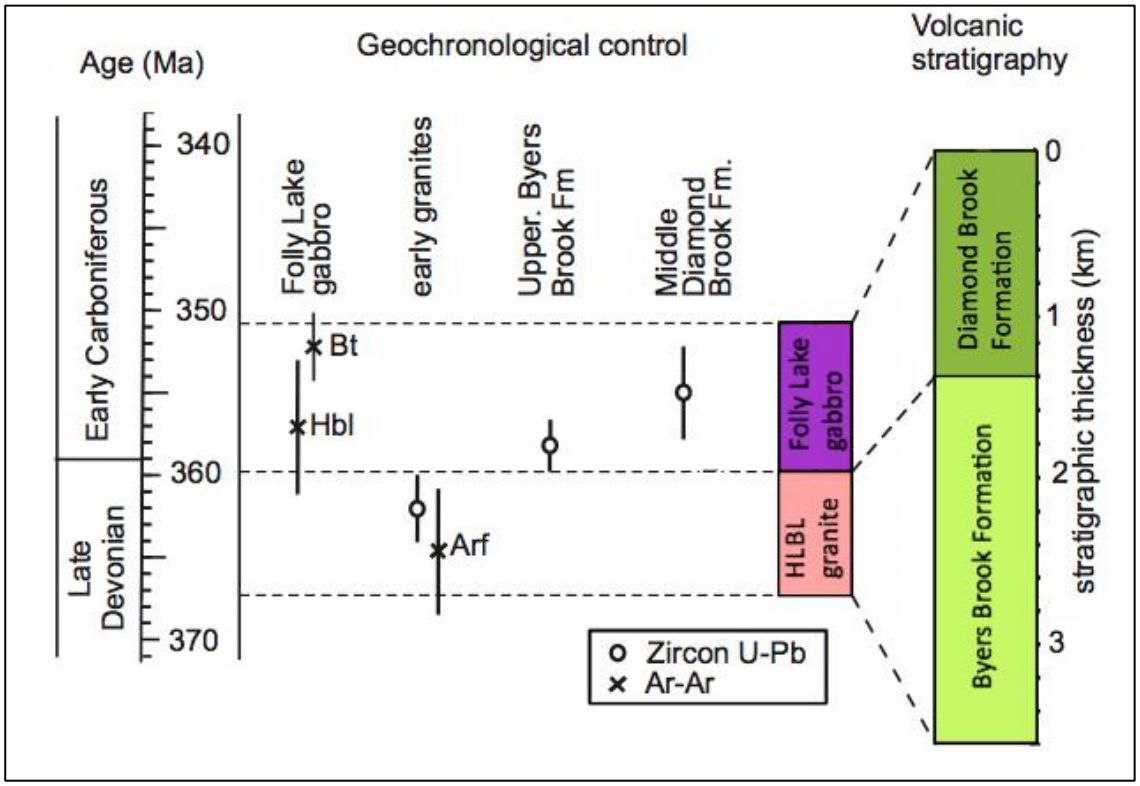

Figure 2.2: Ages of the major magmatic units of the eastern Cobequid Highlands based on geochronchronological controls. U-Pb zircon crystallization ages are from (Doig et al., 1996 and Dunning et al., 2004). Ar-Ar ages on biotite (Bt) and hornblende (Hbl) are from (Pe-Piper et al., 2004) recalibrated as in (Murphy et al. 2011). Diagram modified from (Papoutsa, 2011).

CHAPTER 3: GEOLOGY OF THE DEBERT LAKE AREA

3.1 General geology

The Debert Lake area of Nova Scotia is the location of REE-mineralized dykes (Fig 1.1) and it can be accessed by a NW-SE logging road from the Tatamagouche Wentworth Road. A significant volume of diorite and diabase dykes have intruded the volcanics of the Byers Brook Formation and granitic rocks of the HLBL pluton along the entire length of the NW-SE trending contact (MacHattie, 2011). These mafic magmas are dominantly plagioclase-phyric diorite bodies and diabase dykes and sills (MacHattie, 2011). Within the Debert Lake area, the Byers Brook Formation is dominated by felsic volcanic and volcaniclastic rocks (MacHattie, 2011). There are multiple north-northeast striking subvertical brittle faults that offset the contact between the Byers Brook Formation and the HLBL pluton in this area. As a result of these faults the contact is now offset on a variety of scales between the granite and felsic volcanics. A larger north-northeast striking fault, which separates the rhyolite and granite, named the Big Snare Lake Fault (Fig 4.1), is likely associated with the smaller faults.

3.2 Hart Lake-Byers Lake granite

The HLBL Pluton in the Debert Lake area is comprised of medium to coarse-grained and locally pegmatitic alkali-feldspar granite (MacHattie, 2011; Papoutsa, 2011). The granite contains 50-60% K-feldspar, 25-45% quartz, amphibole, biotite, and Fe-Ti-oxides are the dominant mafic minerals and accessory phases include zircon,

allanite, titanite and epidote (MacHattie, 2011). Some areas of the granite contain phenocrysts of quartz and/or K-feldspar, and some granites display granophyric textures and are interpreted to have crystallized at a shallower depth than the rest of the pluton (Papoutsa, 2011). Enrichment in REE's and rare metals are known to be associated with 'A'-type alkaline granites worldwide (Salvi and Willliams-Jones, 1995; Schmitt et al., 2002; Kerr and Rafuse, 2012). An arfvedsonite-amphibole-bearing and REE-enriched portion of the HLBL pluton was found to occur immediately below the discovery of REE-mineralized granite dykes found within the Byers Brook Formation. This in part suggests a genetic link between this phase of the pluton and REE-mineralization (MacHattie, 2011).

3.3 Rare earth element (REE)-mineralized granite

REE-mineralized granite dykes are located in the Debert Lake area of Nova Scotia at the contact between felsic volcanics of the Byers Brook Formation and alkaline granites of the HLBL pluton (Fig 1.1). Segregated REE-mineralized pods can be found within the arfvedsonite and REE-enriched portion of the HLBL pluton. REE-mineralized alkali-feldspar granite dykes crosscut all other magmatic units in the area (Fig. 3.1). There are two types of REE-mineralized dykes based on grain size, texture and chemistry. Type one dykes are classified as medium-to coarse-grained with a definite "granitic texture" and have noticeably lower concentrations of high field strength elements and rare earth elements compared to the type two dykes. Type two dykes are fine grained and typically exhibit mineralogical banding. Mineralogical compositions of the REE-mineralized dyke samples were determined at Lakehead University Centre for Analytical Services (LUCAS). Modal mineralogy

was determined by back-scattered electron imagery (BSE) and energy dispersive X-ray spectrometry (EDS). Modal mineralogy of the type one REE-mineralized dykes is ~70-75 % quartz, K-feldspar and albite, ~10 % magnetite/hematite, ~10 % epidote and ~5 % zircon, and trace amounts (<5%) of pyrochlore, sphene, monazite, fergusonite, chevkinite, bastanaesite, allanite, ilmenite, yttrialite and fluorite. Type two REE-mineralized dykes have a similar modal mineralogy to the type one dykes with the exception of a higher content of minor and trace minerals and the addition of thorite, thalenite, apatite and calcite(MacHattie, 2011).

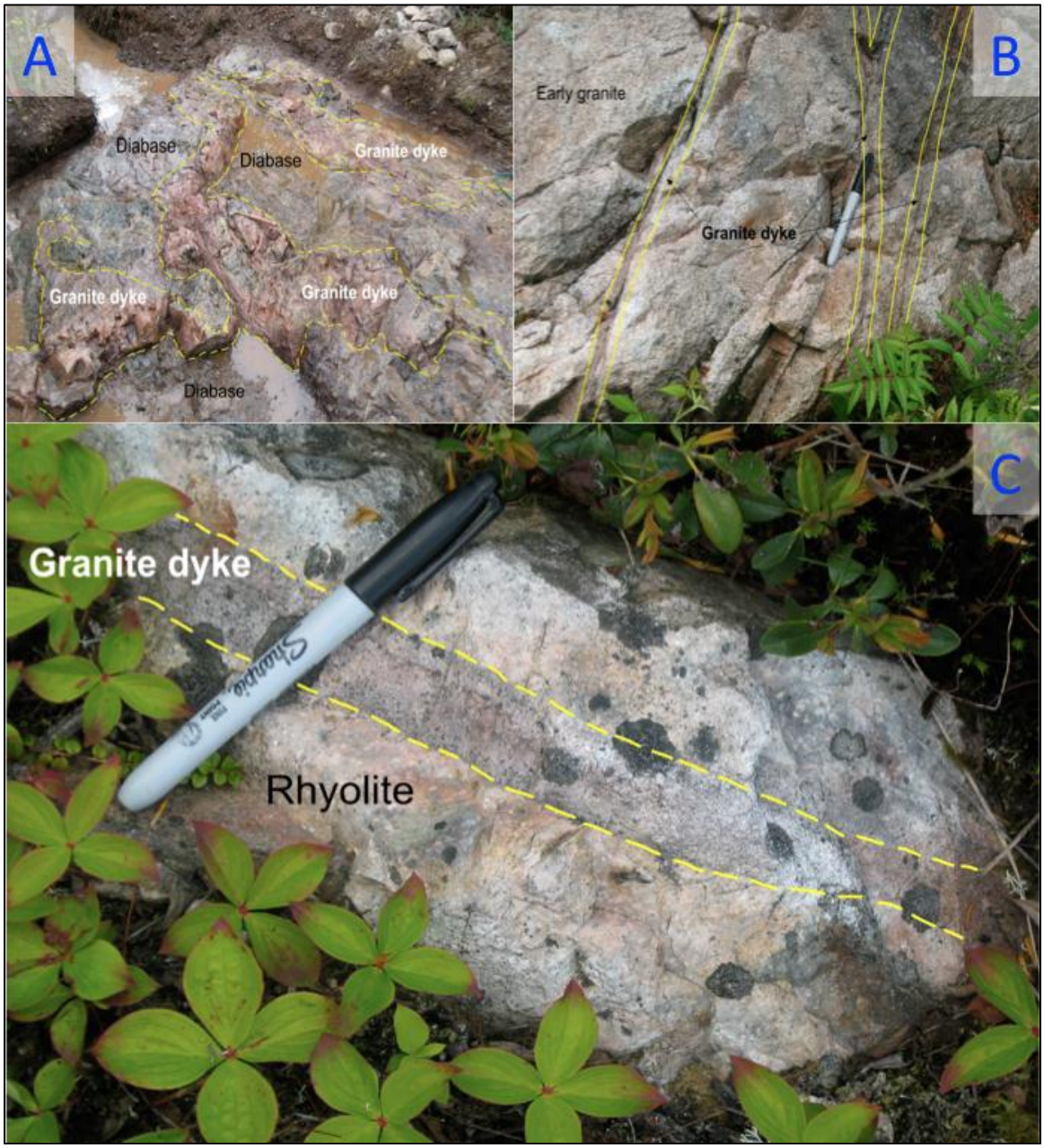

Figure 3.1: REE-mineralized granite dykes cross-cutting A: diabase dyke; B: HLBL granite; C: rhyolite of the Byers Brook Formation. Photos taken by MacHattie (2010).

CHAPTER 4: METHODS

4.1 Previous work on whole rock geochemistry

Mobile x-ray fluorescence (XRF) analyses (> 300) of rock slabs were carried out on granite, diorite and hybrid (between granite and diorite) samples collected throughout the HLBL pluton. These analyses were conducted using the Nova Scotia Department of Natural Resource's mobile XRF X-5000. Each sample was analyzed for three minutes, in three or more random spots, and averages for each sample were tabulated. The data were used to produce geochemical grids for the pluton, and helped to identify specific zones that display greater overall enrichment in HFSE's and REE's (see Fig. 5.1).

Eight samples of the HLBL pluton and seven REE-mineralized granite dyke samples within the Debert Lake area (Fig 4.1) were previously analyzed for major and trace element compositions by fusion inductively couples plasma mass spectrometry (FUS-ICP-MS) and fusion ion-selective electrodes (FUS-ISE) for fluorine concentrations at activation laboratories located in Ancaster, Ontario (MacHattie, 2011). The blue square samples, east of Big Snare Lake, represent the REE-mineralized samples 10TM0024, 10TM0026, 10TM0036, 10TM0049, 10TM0052, 10TM0056, and 10TM0057. The procedures used on each sample are code 4Litho (major and trace elements) and code 4F (fluorine), the methods that follow are found on the labs website (www.actlabs.com). Code 4Litho involves a combination package of lithium metaborate/tetraborate fusion ICP whole rock (Code 4B), giving the major oxides in weight %, and trace element ICP-MS (Code 4B2) in ppm. Code 4F involves taking 0.2 g of each sample, combining it with lithium

metaborate and lithium tetraborate in an induction furnace. This procedure allows for the release of fluoride ions from the sample matrix. After the fuseate is dissolved in dilute nitric acid, a fluoride ion electrode is placed in the solution to directly measure fluoride-ion activity.

4.2 Overview of methods used in this study

This study is being conducted to examine in more detail the relationship between the HLBL granite pluton, a REE-enriched portion of the pluton (defined by a Y-high zone in figure 5.1) and the REE-mineralized granite dykes. The main focus of the study was to characterize amphiboles from the HLBL pluton and from the REE-mineralized dykes to understand how REE concentration to mineralized levels occurred. Petrographic descriptions of each sample were completed to examine any textural and mineralogical differences. Quantitative electron microprobe (EMP) analyses of each sample containing unaltered amphiboles were completed to obtain their geochemistry. Amphiboles are a useful mineral to study because they have a broad chemical composition that closely resembles the bulk composition of the rock (Mitchell, 1990). This will give us a better understanding of the event that caused the emplacement of HFSE-REE-enriched granite dykes in the Debert Lake area and the petrogenesis of the dykes.

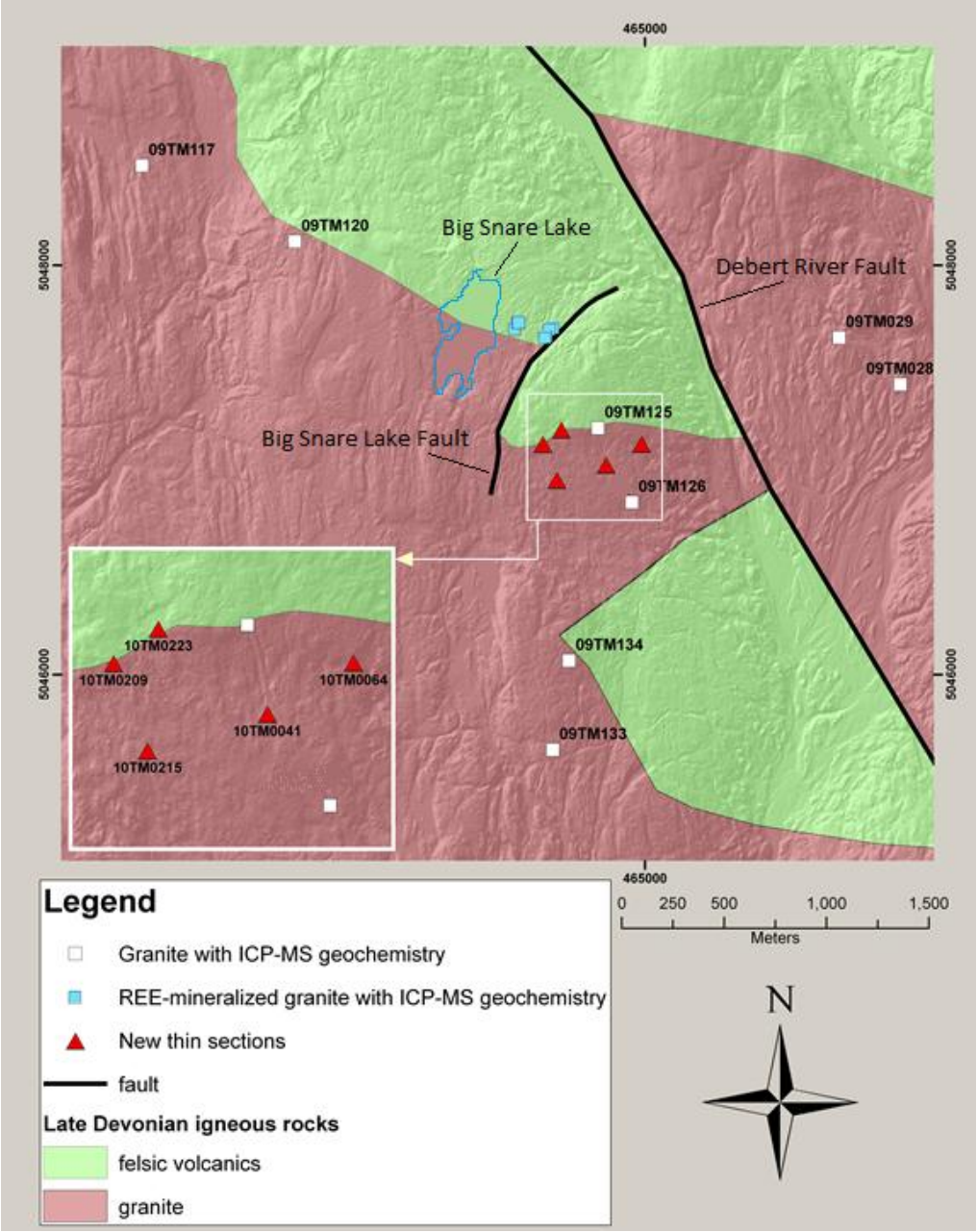

Figure 4.1: Sample distribution. Pink is granite of the HLBL pluton and green is felsic volcanics of the Byers Brook formation.

4.2.1 Petrography

Petrographic descriptions were conducted on samples chosen from each phase of the HLBL granite and on REE-mineralized dykes. Referring to figure 4.1, samples displayed with white and blue squares were previously made into polished thin sections and the samples displayed with red triangles were made into polished thin sections at Dalhousie University for this study. Each sample description was conducted using a Nikon Eclipse 50i petrographic microscope (Fig 4.1 shows the distribution of samples). For each sample modal mineral percent was estimated using a modal percent chart from (Phipotts, 1989). The purpose of petrography in this study was to investigate mineral textures including pleochroism and degree of alteration, primarily in amphibole grains; with follow-up analysis using an EMP. Photomicroscopy was completed to document the textures and mineralogy observed.

4.2.2 Electron microprobe

The JEOL 8200 electron microprobe (EMP) (Fig. 2.2) at Dalhousie University was used to complete quantitative chemical analysis of amphiboles within samples of the HLBL pluton and REE-mineralized granite dykes. Each polished thin section selected was cleaned with an alcohol solution followed by a carbon coating in preparation for EMP analysis. Amphiboles were located using backscatter electron imaging (BSE) and electron dispersive spectroscopy (EDS). There is a moderate contrast between the atomic weight of amphiboles and other minerals found in the granite. Amphiboles have a higher atomic weight than quartz and feldspar but a lower atomic weight than oxides, zircon, and other REE-minerals. Therefore, it was

easy to identify the amphiboles on BSE as being brighter than quartz and feldspar but dimmer than all other minerals. Amphiboles could be distinguished from biotite, similar in brightness on BSE, by cleavage. Sites for analysis were on unaltered, flat surfaces that were chosen using a combination of secondary electron imaging (SEM) and BSE. The number of locations analyzed on each amphibole crystal was chosen based on the size of the amphibole crystal (i.e, larger amphiboles were analyzed at more sites across the crystal to get a better chemical average of that crystal). Standards were calibrated once a week, with peak searches completed each morning.

A suite of 12 elements were used when analyzing the amphiboles. KK (Kaersutite, Kanganui) and sanidine standards were used to calibrate after every 10-20 sample points were picked. The EMP used a voltage of 15kv, amperage of 20nA and beam size of 1μm. Error estimates for quantitative chemical analysis is +/- 2% of the element standards.

Figure 4.2: The JEOL 8200 electron microprobe at Dalhousie University. (Dalhousie earth sciences website)

Chapter 5: RESULTS

5.1: Mobile X-ray fluorescence results

A mobile XRF machine was used to analyze over 300 granite samples from the Hart Lake-Byers Lake pluton. From this data a minimum curvature grid was constructed using Geosoft software on ArcMap to show the relative geochemical distribution of yttrium (Y) in the rocks surrounding the REE-mineralized dykes (MacHattie, 2012; Fig. 5.1). Yttrium, although not a REE, has similar properties as REE's and are often found in association with them (Salvi, 1996). The geochemical grid shows a Y-high zone immediately south and southeast of the REE-mineralized dyke location (blue squares). This defined the extent of the REE-enriched arfvedsonite alkali-feldspar granite that host REE-mineralized pods described earlier in the text.

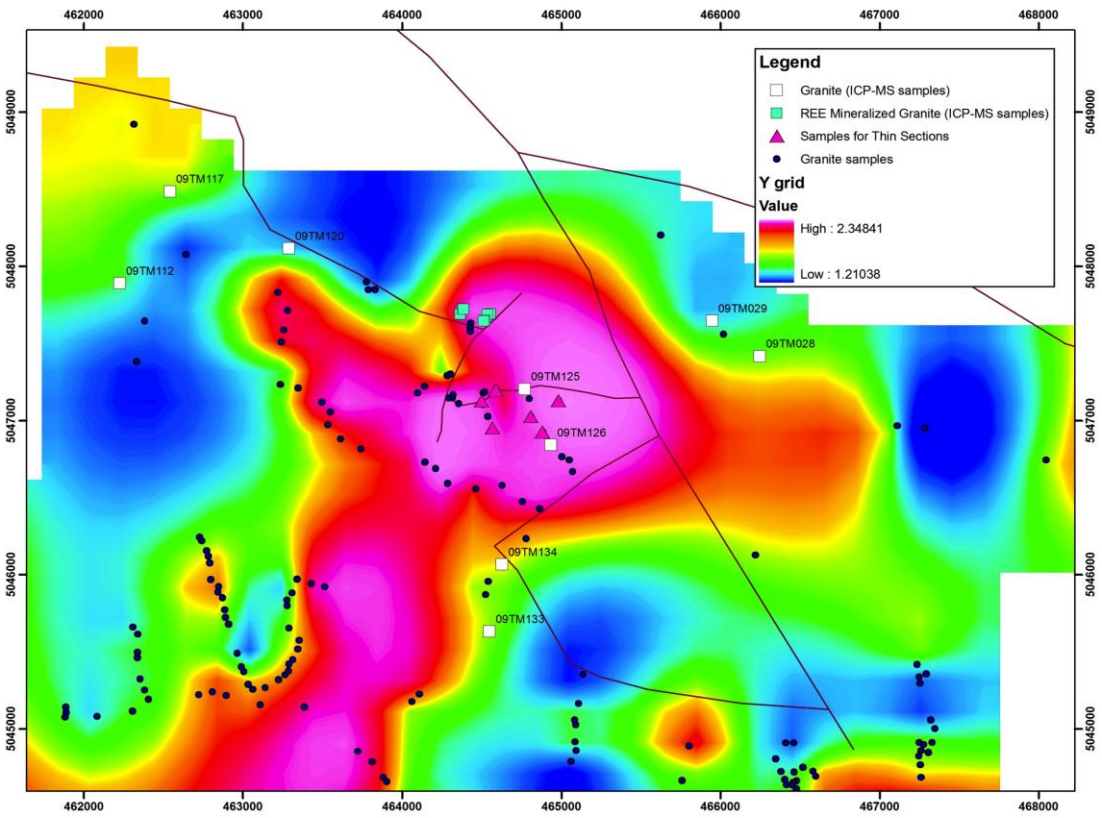

Figure 5.1: Yttrium (Y) geochemical grid for >300 samples (blue squares, some of these areas had more than one sample taken) of the Hart Lake-Byers Lake granite. Analyses of granite were completed using an Olympus Innov-X mobile XRF (X-5000) (MacHattie, 2011).

5.2 ICP-MS results

Fusion ICP-MS data, obtained in 2011, was completed on the blue and white square samples indicated on the sample distribution map (Fig. 4.1). Full ICP-MS and ISE (F) results can be found in Appendix A. The results of these analyses have been plotted on a rare earth element plot (Fig 5.2) and an extended element plot (Fig. 5.3). The type one and type two REE-mineralized dykes described earlier in the text have been combined in these plots for simplicity. The only REE-mineralized dyke sample (10TM0052) that contained amphibole and could be analyzed with the EMP is shown in red on each plot, notice that this sample has the lowest REE-concentrations of the REE-mineralized samples. Granitic rocks of the HLBL pluton possess total REE-concentrations of ~140-360 ppm (n=8), enrichment in light REE's compared to heavy REE's [$(La/Yb)_N$] (table 5.1) and pronounced Eu anomalies. The REE-mineralized dykes have total REE-concentrations ranging from 1800 to >7000 ppm, enrichment in light REE's compared to heavy REE's [$(La/Yb)_N$] (table 5.2) and pronounced Eu anomalies. Based on these results the only major difference between the REE-mineralized dykes and the HLBL pluton is the dramatic increase in REE-concentrations found within the REE-mineralized dykes.

Sample	Sum Gd-Lu/La-Eu (%)	$(La/Yb)_N$
09TM029	27	3.20
09TM028	19	6.03
09TM120	19	4.61
09TM117	14	9.29
09TM134	20	5.57
09TM133	23	3.90
09TM125	24	3.91
09TM126	35	2.59

Table 5.1: Average percent values of heavy rare earth elements (HREE) (Gd-Lu) to light rare earth elements (LREE) (La-Eu) and LREE enrichment of samples from the HLBL pluton (see Fig. 4.1). Samples 125 and 126 are from REE-enriched granite.

Sample	Sum Gd-Lu/La-Eu (%)	$(La/Yb)_N$
10TM0024	39	3.25
10TM0026	53	1.88
10TM0036	21	5.51
10TM0049	70	1.14
10TM0052	36	2.84
10TM0056	23	N/A
10TM0057	155	0.32

Table 5.2: Percent values of heavy rare earth elements (HREE) (Gd-Lu) to light rare earth elements (LREE) (La-Eu) and LREE enrichment of REE-mineralized dyke samples.

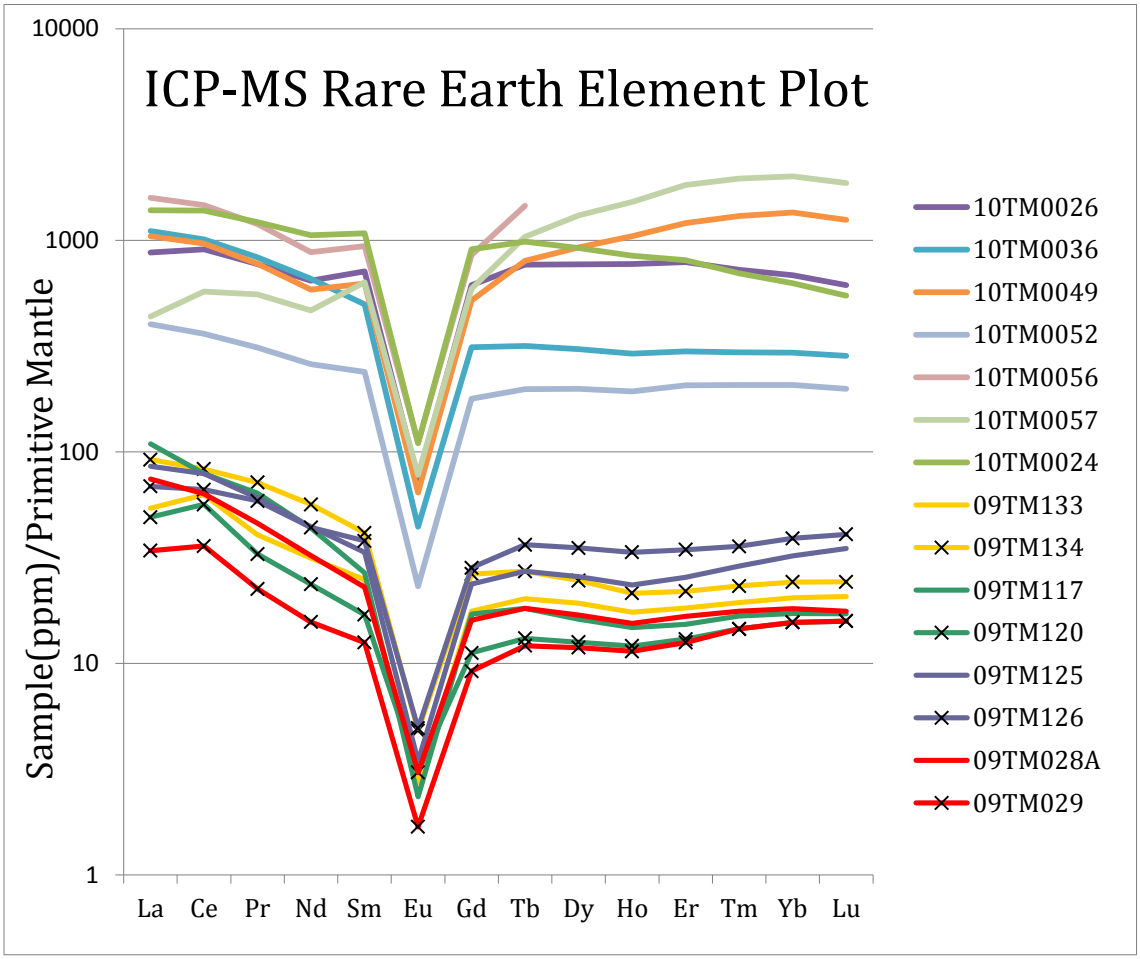

Figure 5.2: Rare earth element plot of Cobequid granitoids normalized to primitive matle (Sun & McDonough, 1989). Modified from MacHattie (2011).

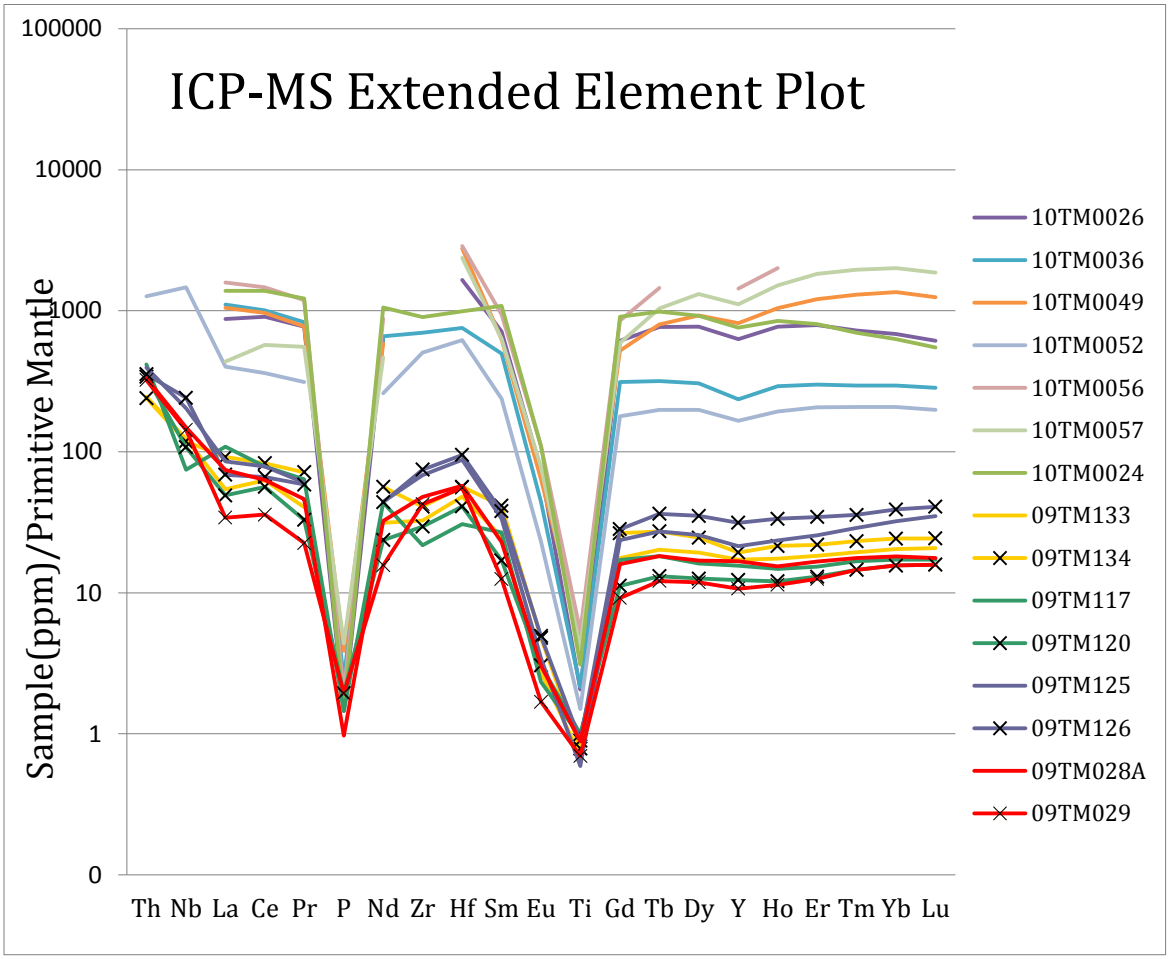

Figure 5.3: Extended element plot of Cobequid granitoids normalized to primitive mantle (Sun & McDonough, 1989). Modified from MacHattie (2011).

5.3 Petrographic observations

Samples labeled in Figure 4.1 as well as REE-mineralized samples, were studied under a petrographic microscope prior to being analyzed with the electron microprobe. Textural observations and modal mineral % of each sample was noted and summarized in Table 5.3 and 5.4. The reason for doing this was to identify the condition and location of amphiboles that were suitable to be analyzed as well as observe alteration textures in the rocks. Samples 09TM133, 09TM134, 09TM117 and 09TM028 and all of the REE-mineralized samples, excluding sample 10TM0052, did not contain amphibole and as a result were not analyzed with the electron microprobe. Micro-veins can be found in most samples of the HLBL-pluton(Fig. 5.4) as well as the REE-mineralized dykes. Epidote veins found in sample 10TM0052 have fluorite crystals associated with them (Fig. 5.5). Nearly all veins are connected to patches of mafic phases throughout the samples, indicating that hydrothermal fluids rich in fluorine likely facilitated the breakdown and partial or complete removal of the mafics. In REE-mineralized sample 10TM0052 relict amphibole can only be found in an area not affected by epidote veining. Under plane polarized light (PPL), amphibole shows pleochroism from greenish brown to yellow within the HLBL granite. Within the REE-enriched granite as well as the REE-mineralized granite dykes the amphiboles display dark blue to black pleochroism (Fig. 5.6).

Sample	Textures	Modal mineral %
09TM028	Equigranular Medium grained altered mafic minerals fluorite around mafics altered feldspar (sericite and clay)	K-feldspar: 55 plagioclase: 5 quartz: 35 mafics: 5
09TM133	granophyric medium-coarse grained quartz and k-feldspar phyric	k-feldspar: 55 plagioclase: 5-10 quartz: 35 mafics: <1
09TM134	some areas granophyric fine-medium grained mafics completely altered veining with flourite	k-feldspar: 55 plagioclase: 5-10 quartz: 35 mafics: <1
09TM117	Equigranular Fine-medium grained amphibole altered, opaques associated with mafics feldspars very altered (sericite and clay)	k-feldspar: 45 plagioclase: 10-15 quartz: 35 mafics/oxides: 5

Table 5.3: Petrographic descriptions of HLBL-granite samples that do not contain amphibole. Mafics include amphibole, biotite, and Fe-Ti oxides.

Sample	Textures	Modal mineral %
09TM029	Equigranular Fine-medium grained Mafics altered, not as much as in 28A <1mm zircons crystals associated with mafics Altered feldspar (sericite and clay)	K-feldspar: 55 plagioclase: 5 quartz: 35 mafics:5
09TM120	Fine-med grained Equigranular Altered feldspar (sericite and clay) Amphiboles- green-yellow (one patch); brown and green amphiboles are altered	K-feldspar: 55 plagioclase: 10 quartz: 30 mafics: 3
10TM0041	Equigranular Medium grained Green and blue pleochroic amphiboles	K-feldspar: 50 plagioclase: 0 quartz: 40 mafics: 10
10TM0064	Equigranular Medium grained Green to blue pleochroic amphiboles	K-feldspar: 45 plagioclase: 5 quartz: 40 mafics: 10
10TM0125	Fine-coarse grained Pegmatitic Altered feldspar (pinkish brown in ppl) Very big amphibole, deep blue to grey-blue pleochroism	K-feldspar: 55 plagioclase: 0 quartz: 35 mafics: 10
10TM0209	Equigranular Medium grained Some areas granophyric Brownish green or black to blue pleochroic amphiboles	K-feldspar: 55 plagioclase: <5 quartz: 35 mafics: 5
10TM0215	Granophyric Yellow green-brown or black to blue pleochroic, 10mm long amphibole Very weathered feldspars (sericite and clay)	K-feldspar: 55 plagioclase: <5 quartz: 35 mafics: 10
10TM0223	Equigranular Fine grained Yellow green-brown to deep blue pleochroic	K-feldspar: 55 plagioclase: <5 quartz: 40 mafics: 5
10TM0052	Epidote veins, alteration and partial removal of mafic minerals around veins Flourite crystals associated with epidote veins Most amphiboles altered to fine grain biotite, where not altered deep blue-black pleochroism	K-feldspar: 60 plagioclase: <1 quartz: 35 mafics: 5

Table 5.4: Petrographic descriptions of samples that do contain amphibole. Mafics include amophibole, biotite and Fe-Ti oxides.

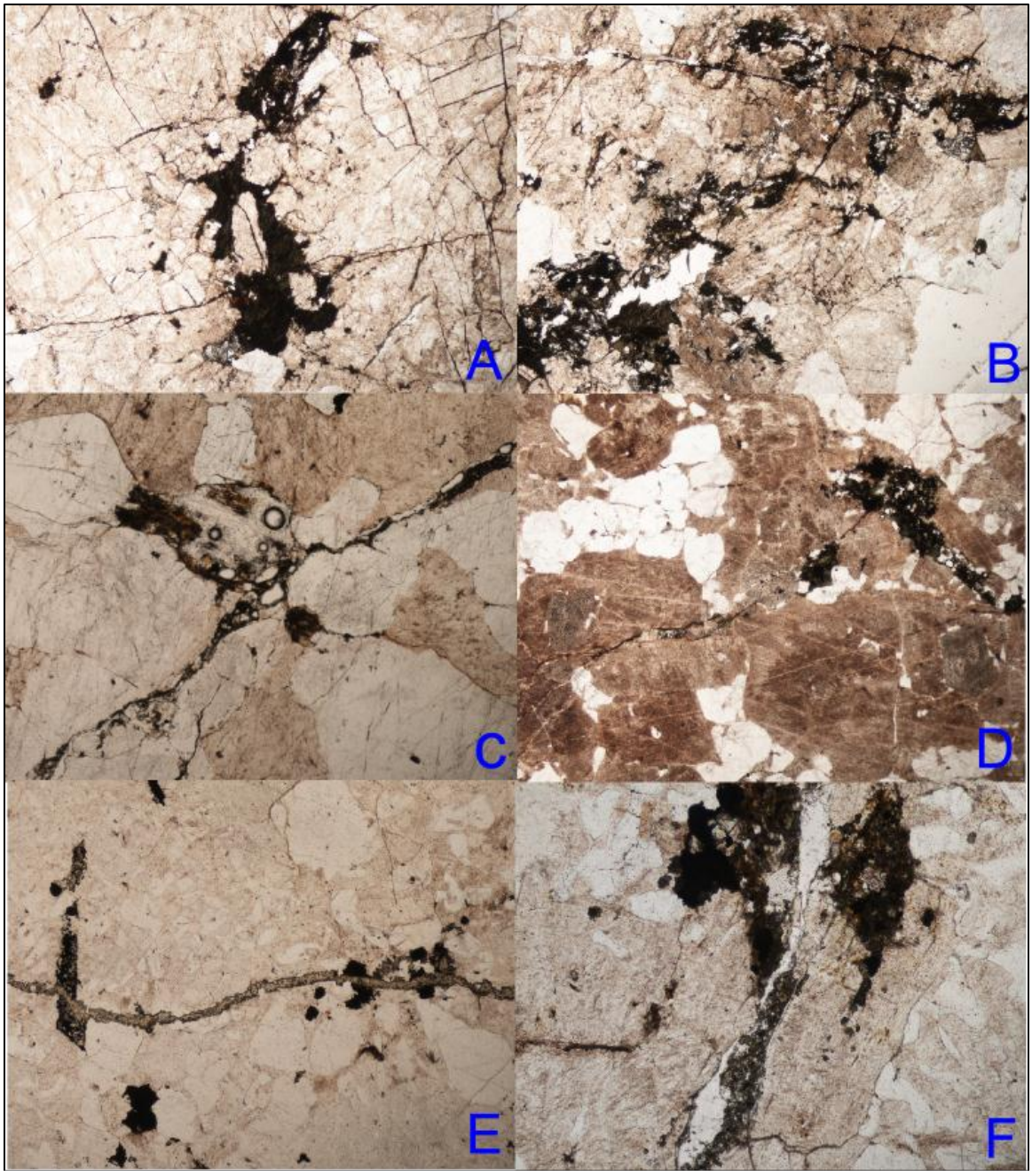

Figure 5.4: Photomicroscopy of micro-fractures in plane polarized light(PPL) partially or completely filled with epidote ± fluorite in A: Sample 09TM028 FOV: 2.5mm; B: Sample 09TM028 FOV: 6.25mm; C: Sample 09TM134 FOV: 1.25mm; D: Sample 09TM117 FOV: 6.25mm; E: Sample 09TM133 FOV: 2.5 and F: Sample 09TM134 FOV: 6.25

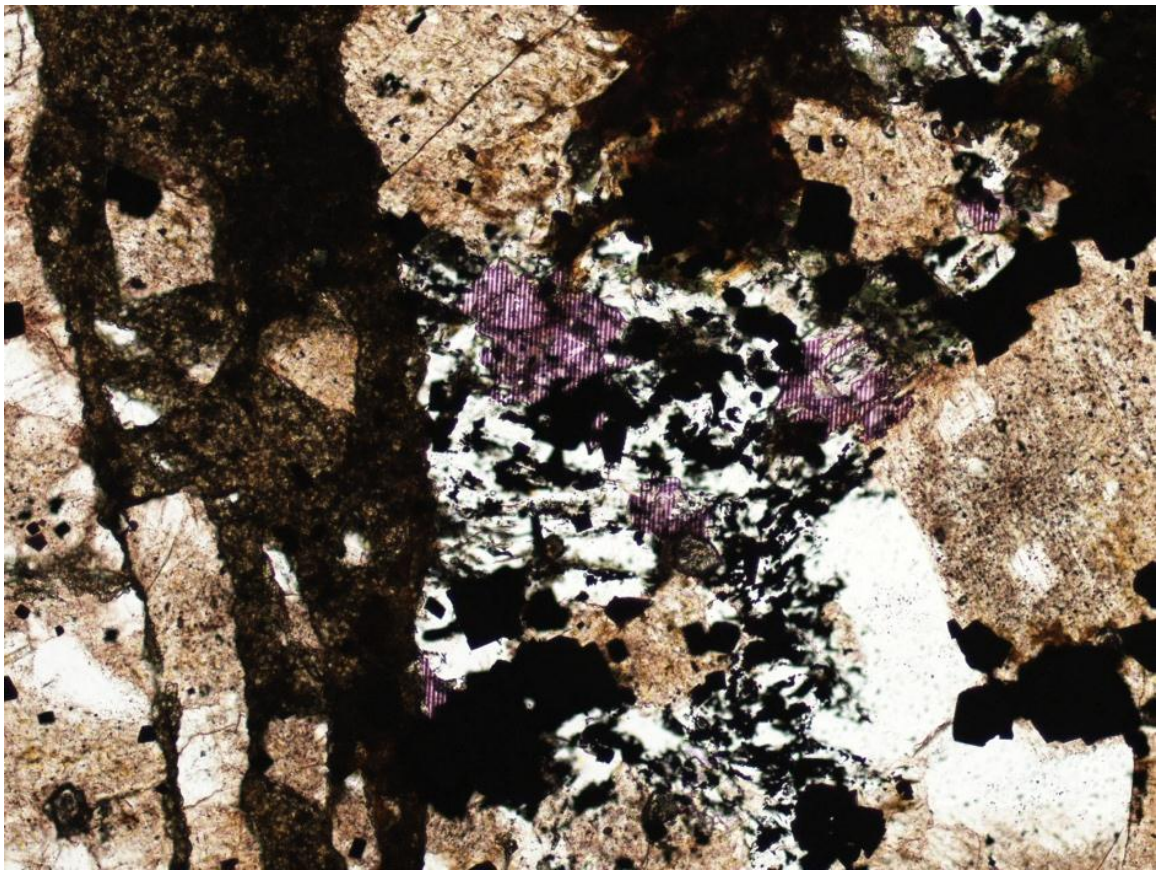

Figure 5.5: Epidote vein with fluorite crystals in REE-mineralized sample 10TM0052, FOV: 1.25mm, PPL.

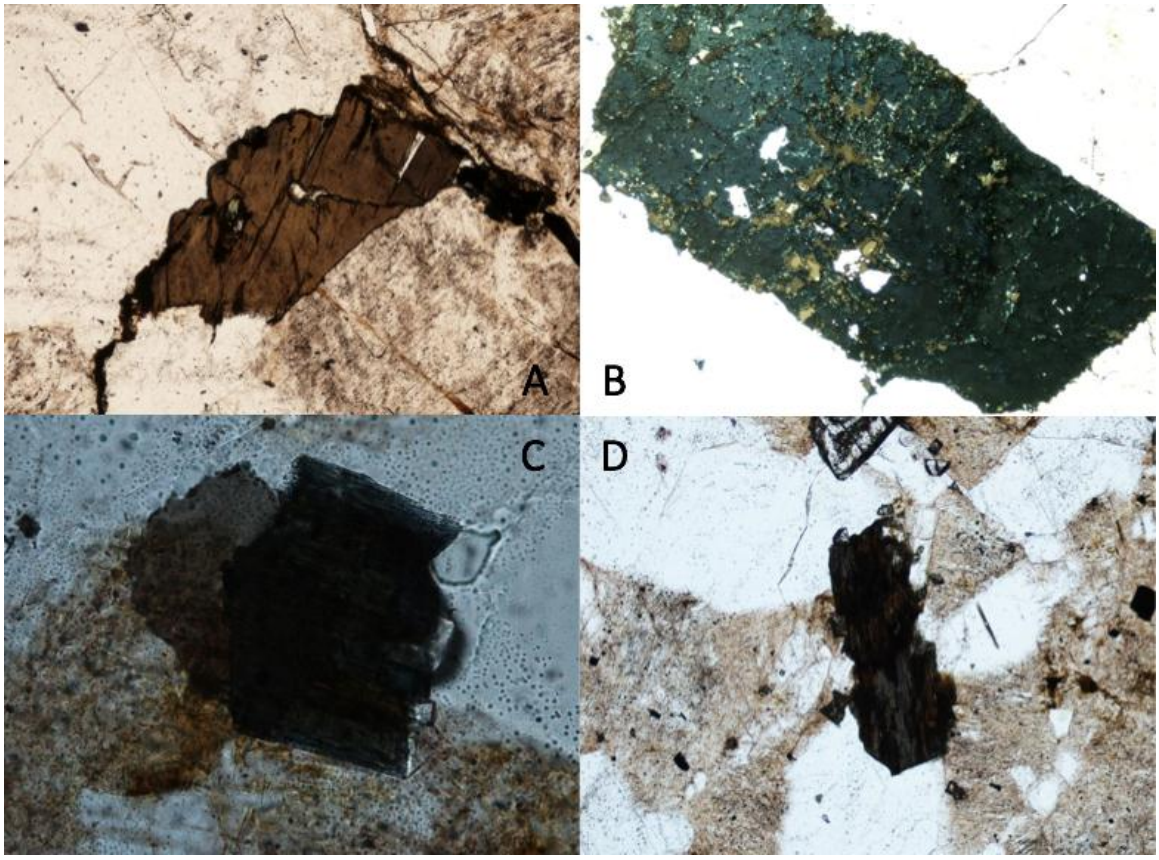

Figure 5.6: Photomicroscopy of amphibole grains showing color of pleochroism from A: HLBL granite from sample 09TM120FOV=2.5mm, B: REE-enriched arvedsonite granite from sample 10TM0125 FOV=6.25mm, C and D: REE-mineralized dyke sample 10TM0052 FOV= 0.25mm and 1.25mm respectively. All photos in PPL.

5.4: Amphibole geochemistry

Electron microprobe results are found in appendix B along with BSE images of amphiboles and a representation of analysis points. The results were converted from oxides to formula units and plotted on classification diagrams by Leak et al. (1997) to determine the amphibole name. To determine which amphibole diagram to emply (e.g distinguish between calcic, sodic-calcic, or sodic amphiboles) the diagram parameters first had to be met. After determining the diagram parameters Mg / (Mg + Fe) was plotted against silica content in the formula. Amphibole from samples 09TM120 and 09TM029 fit the chemical parameters of a sodic-calcic amphibole [(Na + K) ≥ 0.50; (Ca + Na) ≥ 1.00; 0.50 < Na < 1.50] (Fig. 5.7). Both samples have amphiboles that plot as kataphorite [6.5-7.5 Si in formula and 0-0.5 Mg/ (Mg + Fe)]. Amphibole from samples 09TM125, 09TM126, 10TM0209, 10TM0223, 10TM0041, 10TM0064, 10TM0215, and REE-mineralized dyke sample 10TM0052 fit the chemical parameters of sodic amphiboles [Na ≥ 1.50; (Mg + Fe + Mn) > 2.5; (Al or Fe) > Mn; Li < 0.5; (Mg or Fe) > Mn and (Na + K) ≥ 0.50]. The sodic amphiboles all plot as arfvedsonite [7.5-8 Si in formula and 0-0.5 Mg/ (Mg + Fe)] (Fig. 5.8). The high silica content (some that show >8) is likely due to other elements in the amphibole that were erroneously included in the analysis. These results demonstrate that there are clearly two very different groups of amphiboles present in the HLBL granites. The REE-mineralized granite dykes have arfvedsonite amphibole with the same chemical signature as the arfvedsonite-bearing REE-enriched granitoids recognized previously by MacHattie (2011). Harker variation

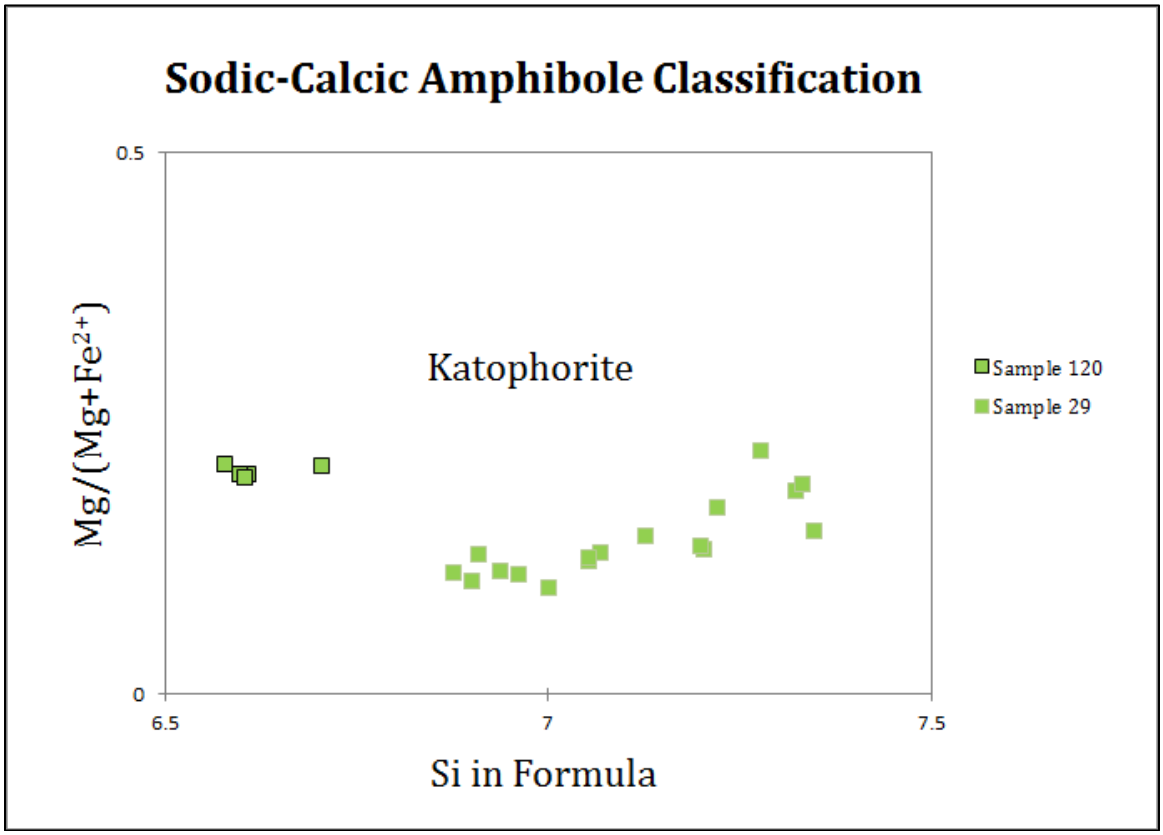

Figure 5.7: Classification of the amphibole from samples 09TM120 and 09TM029 based on nomenclature of amphiboles from Leak (1997). Diagram parameters: (Na + K) ≥ 0.50; (Ca + Na) ≥ 1.00; 0.50 < Na < 1.50.

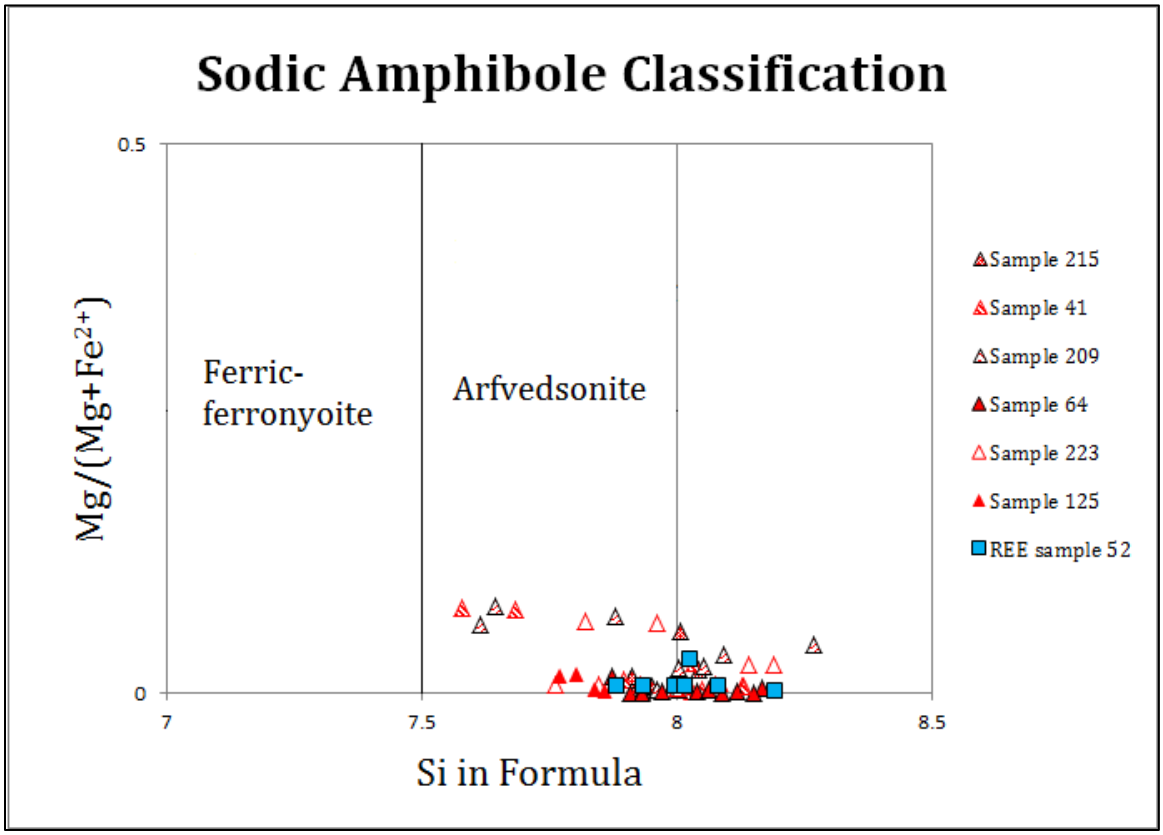

Figure 5.8: Classification of the amphibole from samples 09TM120 and 09TM029 based on nomenclature of amphiboles from Leak (1997)

are shown on Figure 5.9 for the major elements and on Figure 5.10 for minor elements. The sample symbols used on the variation diagrams match the sample symbols on the classification diagrams (Fig. 5.7 and 5.8). With a first glance at these diagrams we can notice there are distinctly two different geochemical groups in the HLBL granite. One group includes kataphorite amphiboles (green squares) of the HLBL pluton and the other group includes arfvedsonite amphiboles from the REE-mineralized dyke (blue squares) and REE-enriched granitoids (variable red triangles). Some trends are apparent within each group including TiO2, Al2O3, MgO and CaO suggesting some chemical fractionation processes are occurring within these rocks. Scatter is normal in these diagrams and is caused by a combination of analytical error and chemical variations in the rocks that occur naturally. On the variation diagram that displays TiO_2 vs. SiO_2 the kataphorite and arfvedsonite amphibole groups both have trends of decreasing TiO_2 with increasing SiO_2 that are nearly the same, in terms of TiO_2 content. Similarly with diagrams of CaO, Na_2O, K_2O, and MnO versus silica the two separate amphibole groups clearly follow separate evolutionary paths. MgO vs. SiO_2 shows separate trends for HLBL samples 09TM120 and 09TM029, which are from opposite sides of the REE-enriched granite zone (see fig. 5.10). Al_2O_3 vs. SiO_2 is the only variation diagram with a smooth trend. The trace element variation diagrams vs. SiO_2 content all show variable amounts of trace elements or oxides vs. SiO_2 content with no obvious trends.

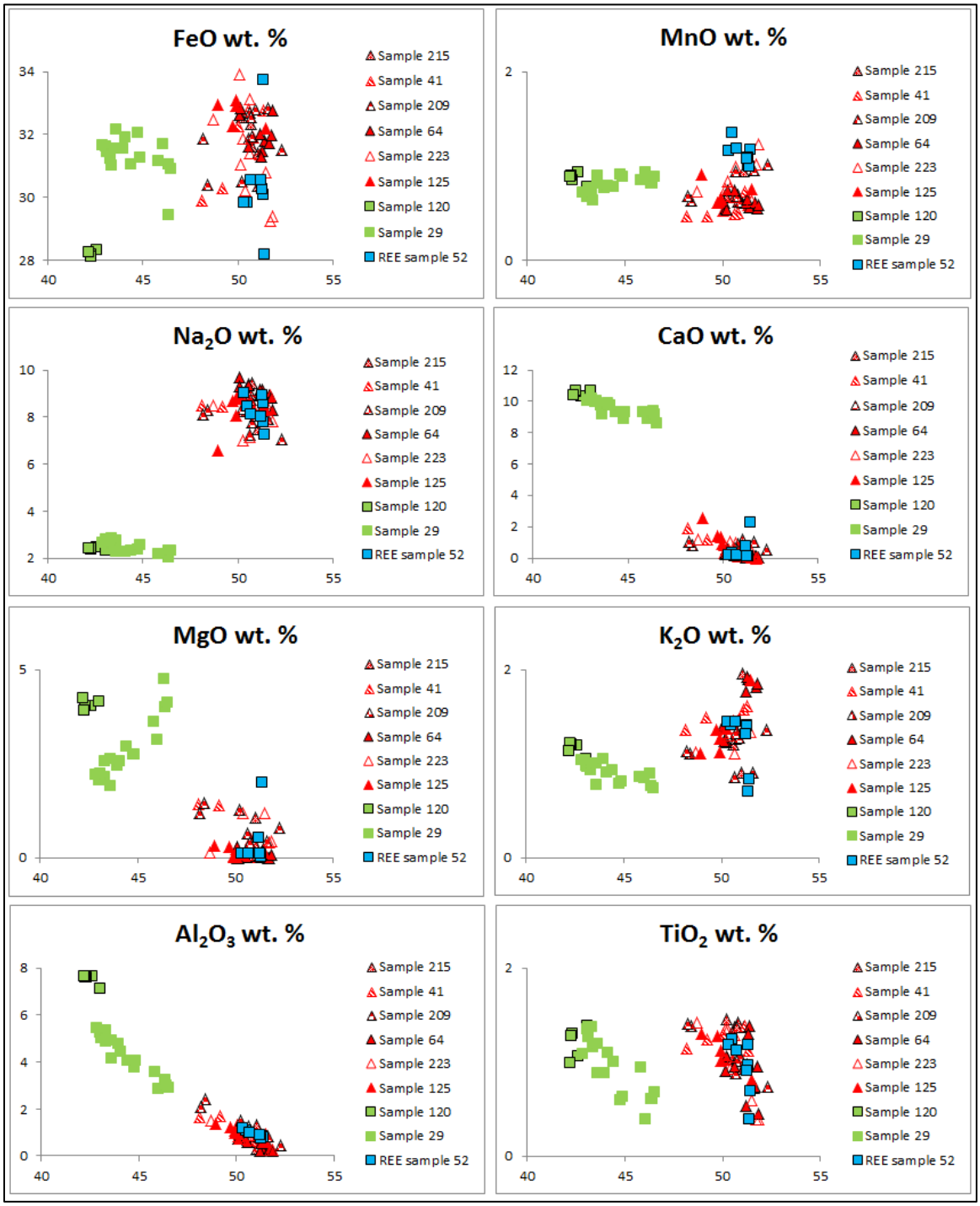

Figure 5.9: Harker variation diagrams, using electron microprobe (EMP) results of amphiboles (Appendix B), showing the relationship between major oxides vs. SiO_2 (wt. %).

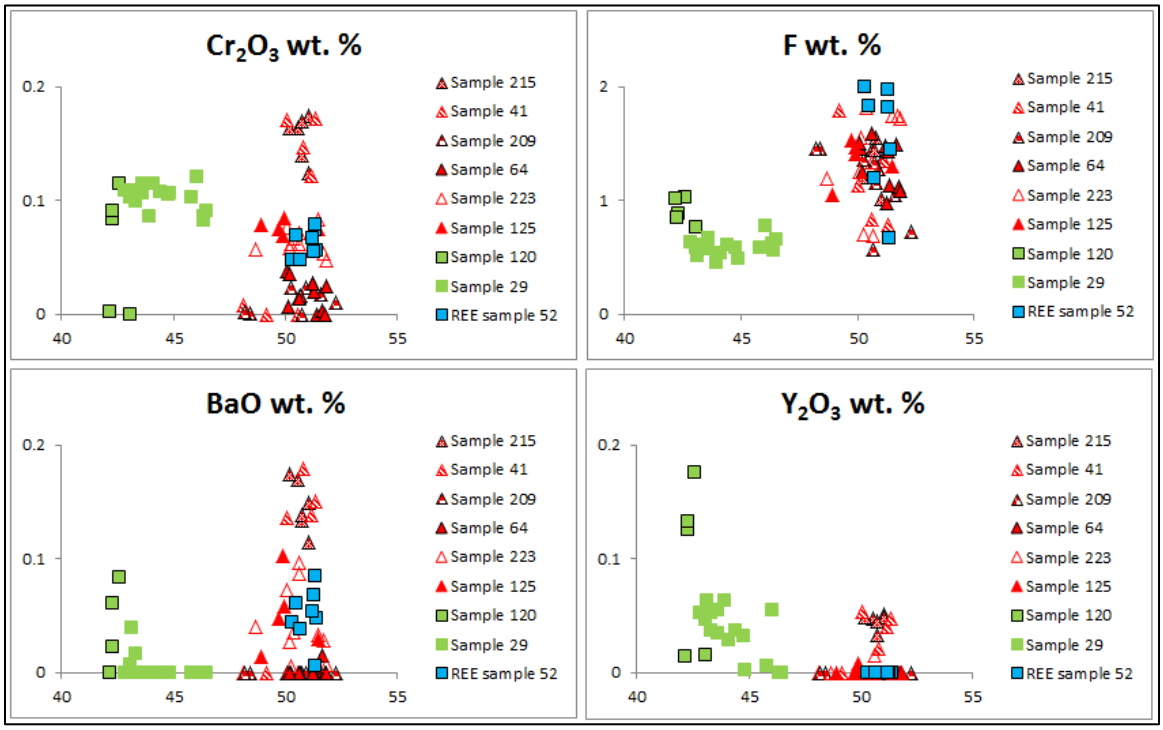

Figure 5.10: Harker variation diagrams, using electron microprobe (EMP) results of amphiboles (Appendix B), showing the relationship between minor oxides and elements vs. SiO_2 (wt. %).

To examine more closely chemical variations within the arfvedsonitic amphibole Figure 5.11 shows all the major oxides vs. silica on the abscissa and figure 5.12 shows all the minor oxides and fluorine (F) vs. silica. In figure 5.11 trend lines with R^2 values were placed on any graph that looked to have a reasonable trend. The R^2 value represents how well the oxide can be predicted by the silica content and vice versa. An R^2 value of 1 indicates that the oxides on the diagram perfectly predict each other, and an R^2 value of 0 would mean they can't be predicted by each other. FeO, Na_2O and MgO vs. SiO_2 in figure 5.11 likely have R^2 values very near 0 since there doesn't appear to be any obvious trends visible on the plots. The rest of the oxides vs. SiO_2 show some chemical trends, especially Al_2O_3, TiO_2 and K_2O with R^2 values above 0.5. CaO, Al_2O_3 and TiO are all decreasing with increasing SiO_2. K_2O, and MnO are increasing with increasing SiO_2.

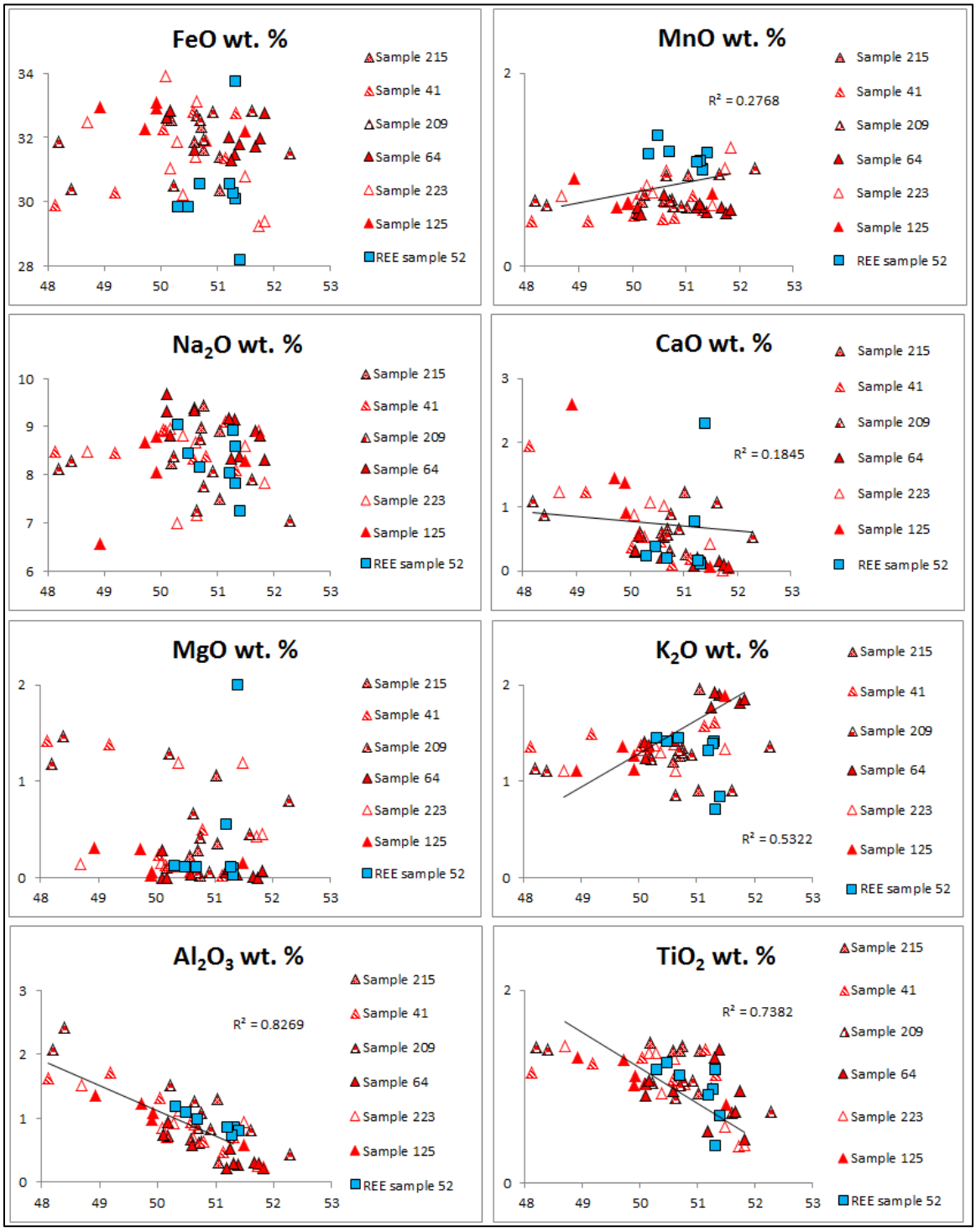

Figure 5.11: Harker variation diagrams, using electron microprobe (EMP) results of arfvedsonite amphiboles (Appendix B), showing the relationship between major oxides vs. SiO2 (wt. %).

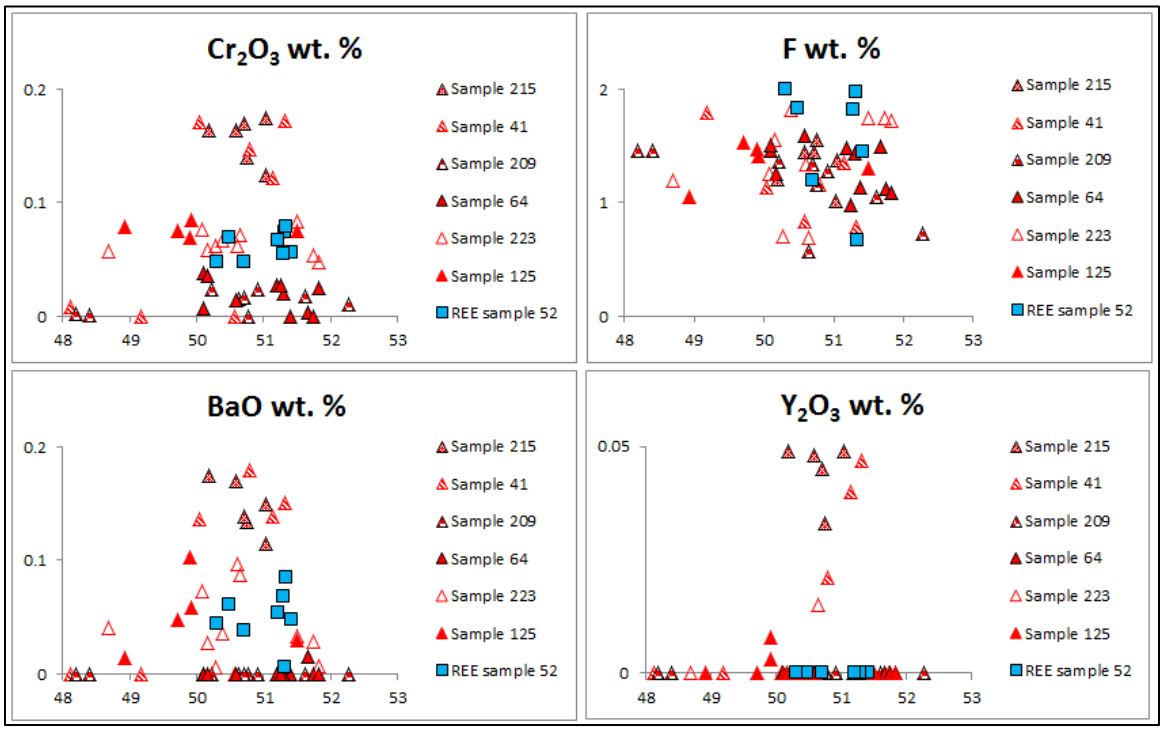

Figure 5.12: Harker variation diagrams, using electron microprobe (EMP) results of arfvedsonite amphiboles (Appendix B), showing the relationship between minor oxides and F vs. SiO2 (wt. %).

CHAPTER 6: DISCUSSION

6.1: Introduction

Amphiboles have proven to be a useful mineral to analyze when studying geochemical trends of alkaline igneous complexes (Mitchell, 1990). Amphiboles have a broad chemical range which closely reflects whole rock chemistry. Amphibole chemistry in this study was used to examine geochemical similarities and differences between the HLBL pluton, REE-mineralized granite dykes and REE-enriched granite containing REE-mineralized segregated pods, as defined earlier by MacHattie (2011).

6.2: Whole rock geochemistry

Geochemical grids were constructed from mobile XRF analyses of rock slabs from the HLBL and REE-mineralized dykes in previous work conducted by MacHattie (2011). A geochemical grid of yttrium (Y) concentrations (Fig. 5.2) shows there are high concentrations of Y linked with the REE-mineralized dykes and REE-enriched granitoid compared to the rest of the HLBL pluton. These results gave an indication that the REE-mineralized granite may be genetically related to the REE-enriched granitoid, discovered immediately south and southeast of the REE-mineralized dykes and hosting REE-mineralized pods. Fusion ICP-MS analysis was completed on eight samples of the HLBL pluton and seven REE-mineralized granite dyke samples within the Debert Lake area (Fig 4.1) for major and trace element compositions, including REE's and fluorine. Based on the fusion ICP-MS results samples from the HLBL granite show enrichment in light REE's(LREE) compared to

heavy REE's(HREE) ($(La/Yb)_N$) compared to samples from the REE-mineralized dykes which show an overall depletion in $(La/Yb)_N$ (Table 5.1 and 5.2) and REE-enriched granite. The HLBL samples show overall lower proportions of HREE's relative to LREE's (sum Gd-Lu/La-Eu) compared to REE-mineralized granite. The REE-enriched arfvedsonite granite has $(La/Yb)_N$ and (sum Gd-Lu/La-Eu) values that are more similar to the REE-mineralized granite. On a mantle-normalized REE-plot the granitic rocks of the HLBL pluton show similar patterns as the REE-mineralized granite, both have pronounced Eu anomalies but the HLBL granite has a noticeable enrichment in LREE compared to HREE that isn't as apparent in the REE-mineralized granite. Overall chemical patterns for the trace elements in the REE-mineralized dykes, REE-enriched granite and HLBL-pluton are all very similar, suggesting they came from a similar source.

6.3: Amphibole chemistry

EMP results were converted from weight percent to formula units to classify the type of amphiboles present in the samples. The results determined kataphorite amphiboles are present immediately outside of the Y-high zone and arfvedsonite amphiboles are present in the REE-enriched and REE-mineralized granite. Kataphorite amphibole is lower in Si, Fe, and Na and higher in Al, Mg and Ca compared to arfvedsonite amphibole. This change in chemistry in the amphiboles suggests the arfvedsonite amphiboles may have resulted from fractional crystallization of the HLBL pluton, where we would expect to see enrichment in Fe, Na, Si and REE in the latest melt. The results of major and trace oxides plotted on Harker variation diagrams (Fig. 5.10 and 5.11) prove that fractional crystallization

from the HLBL parental magma is not the process that caused REE-concentration into REE-mineralized dykes. The diagrams show that there are two separate chemical trends resulting from the two different types of amphibole, which suggests the REE-mineralized and REE-enriched granite did not fractionate from the HLBL-pluton upon cooling. Since the arfvedsonite amphibole chemistry between the REE-mineralized dykes and REE-enriched granitoids are so similar (Fig. 5.12 and 5.13) it is very likely that they are genetically related to each other. Comparing the REE-mineralized dyke and REE-enriched granitoid (Fig. 5.12 and 5.13) there does not appear to be any major variations in chemistry. This strongly suggests that fractional crystallization of the arfvedsonite granite magma had very little effect in concentrating REE's in the REE-mineralized dykes. The extreme concentration of REE's in the dykes compared to the REE-enriched granitoid may be due to fluids in the arfvedsonite granite intrusion being rich in fluorine and possibly chlorine (Table 6.1) , which are known to keep REE's in solution (Salvi, 1996). The reason why that there is little evidence of magma differentiation between the REE-enriched granite (which would have crystallized earlier) and the REE-mineralized dykes (a result of expulsion of the last melt in the intrusion) is likely due to the intrusion already being extremely alkaline to begin with, leaving very little room for differentiation.

Sample	ISE F data (wt. %)	Sample	Sum EMP F data wt. %
09TM028	0.14	10TM0215	1.34
09TM029	0.01	10TM0041	1.30
09TM117	0.05	10TM0209	1.15
09TM120	< 0.01	10TM0064	1.32
09TM133	< 0.01	10TM0223	1.37
09TM134	< 0.01	09TM125	1.35
09TM125	0.07	10TM0052	1.55
09TM126	0.05	09TM120	0.91
10TM0024	0.08	09TM029	0.59
10TM0026	0.19		
10TM0036	0.38		
10TM0049	1.36		
10TM0052	0.23		
10TM0056	0.06		
10TM0057	0.29		

Table 6.1: Fluorine content variation between HLBL granite, REE-enriched granite, and REE-mineralized granite. Data from FUS-ISE analysis (MacHattie, 2011) and EMP amphibole analysis. Sample distribution can be found in figure 4.1.

CHAPTER 7: CONCLUSIONS AND RECOMMENDATIONS

7.1: Conclusions

REE-mineralization in the Debert Lake area of Nova Scotia is found in alkali feldspar granite dykes that cross-cut all other magmatic units in the area. The REE-mineralization is spatially associated with the HLBL pluton, which is a peralkaline to peraluminous granite pluton. Immediately south and southeast of the REE-mineralized dykes is a REE-enriched arfvedsonite bearing alkali feldspar granite.

1. ICP-MS results suggest that the REE-mineralized dykes and HLBL granite either come from separate sources or the REE-mineralized dykes have differentiated from the HLBL granite. The HLBL granite show enrichment in light LREE's relative to heavy HREE's ($(La/Yb)_N$) compared to the REE-mineralized dykes and REE-enriched granite (Table 5.1 and 5.2). In addition, the HLBL samples show overall lower proportions of HREE's relative to LREE's (sum Gd-Lu/La-Eu) than REE-mineralized and REE-enriched granite. The REE plot (Fig. 5.2) and extended element plot (Fig. 5.3) of the ICP-MS data show overall similar patterns for the HLBL pluton, REE-enriched and REE-mineralized granite suggesting they may be genetically related to each other or come from similar sources.

2. EMP results solidify that the REE-enriched granite did not form as a result of fractional crystallization of the HLBL-pluton. Granitic rocks of the HLBL-pluton that surrounds the REE-enriched granite contain kataphorite amphibole, and the REE-enriched granite contains arfvedsonite amphibole (Fig 5.8 and 5.9). Harker variation diagrams of all samples (Fig. 5.10 and 5.11) give a visualization of geochemical trends occurring in the granite. The kataphorite amphibole of the HLBL

granite are following separate geochemical trends from the arfvedsonite amphibole, with a silica gap between each type of amphibole suggesting they did not fractionate from one homogenous magma chamber. Variation diagrams with only the arfvedsonite amphibole (Fig. 5.12 and 5.13) show that there are no significant chemical difference between the REE-enriched granite and REE-mineralized granite suggesting crystal fractionation had little play in the concentration of REE's.

3. Based on ICP-MS combined with EMP results the REE-mineralized granite is genetically associated with the REE-enriched granite, both of which are distinctly more enriched in HFSE and REE compared to the majority of the HLBL granite pluton. ICP-MS and EMP results show an enrichment in fluorine within the REE-mineralized dykes compared to the REE-enriched and HLBL granite. These data could suggest compositional differenced existed in the source region(s) for the HLBL-pluton and/or that the conditions of melt generation may have been varied.

7.2: Recommendations

My first recommendation would be to get a larger sample size across the field area to really define each phase of granite. The geochemical trends presented in this thesis are limited due to limited amphibole data, if there were more samples and more data from each phase (REE-mineralized dykes, REE-enriched granite and HLBL granite) perhaps we would see some trends that are not apparent as of now. My second recommendation would be to obtain geochronological ages of each phase to quanitify when they were emplaced relative to one another. A third recommendation would be too study more closely the fractionation of Y and REE's

in this fluorite-precipitating hydrothermal system, much like a study by Bau (1995),

to really understand the movement of REE's and how they were concentrated.

REFERENCES

Actlabs.com. Methods Retrieved from: http://www.actlabs.com/list.aspx?menu=64&app=226&cat1=549&tp=12&lk=no

Bau, M., Dulski, P., 1995: Comparative study of yttrium and rare-earth element behaviours in fluorine-rich hydrothermal fluids. Contrib Mineral Petrol, v.119, p. 213-223.

Boily, M., Williams-Jones, A. E., 1994: The role of magmatic and hydrothermal processes in the chemical evolution of the Strange Lake pluton complex, Quebec-Labrador. Contrib Mineral Petrol, v. 118, p. 33-47.

Calder, J. H., 1998: The Carboniferous evolution of Nova Scotia. Geological Society of London, Special Publication, v. 143, p. 261-302.

Castor, S. B., Hendrick, J. B., 2006: Rare earth elements. Industrial Minerals and Rocks: Commodities, Markets, and uses, 7th edition. SME. P1568

Davies, S., 2010: Applications of the Rare Earth Elements. Chemistry @suite 101

Doig, R., Murphy, J. B., Pe-Piper, D. J., 1996: U-Pb geochronology of Late Paleozoic plutons, Cobequid Highlands, Nova Scotia, Canada: evidence for Late Devonian emplacements adjacent to the Meguma-Avalon terrane boundary in the Canadian Appalachians. Geological Journal, v. 31, p. 179-188.

Donohoe, H. V., Wallace, P. I., 1982: Geological map of the Cobequid Highlands, Nova Scotia. Scale 1:50000. Nova Scotia Department of Mines and Energy.

Dunning, G. R., Barr, S. M., Giles, P. S., McGregor, D. C., Pe-Piper, G., Piper, D. J. W., 2002: Chronology of Devonian to early Carboniferous rifting and igneous activity in southern Magdalen Basin based on U-Pb (sircon) dating. Canadian Journal of Earth Sciences, v. 29, p. 1219-1237.

Hicks, R.J., Jamieson, R. A., and Rynolds, P. H, 1999: Detrital and metamorphic 40Ar/39Ar ages from muscovite and whole-rock samples, Meguma Supergroup, southern Nova Scotia. Canadian Journal of Earth Sciences, v. 36, p. 23-32.

Keppie, J. D., Dalmeyer, R. D., 1987: Dating transcurrent terrane accretion: an example from the Meguma and Avalon composite terranes in the northern Appalachians. Tectonics, v. 6, p. 831-847.

Kerr, A., Rafuse, H., 2012: Rare-earth element (REE) geochemistry of the Strange Lake deposit: implications for resource estimation and metallogenic models. Geological Survey, report 12-1, p. 39-60.

Koukouvelas, I., Pe-Piper, G., Piper, D. J. W., 2006: The relationship between length and width of plutons, within the crystal-scale Cobequid Shear Zone, northern Appalachians, Canada. Earth Sciences, v. 95, p. 963-976.

Leak, B. E., et al., 1997: Nomenclature of amphiboles: report of the subcommittee on amphiboles of the international mineralogical association, commission on new minerals and mineral names. The Canadian Mineralogist, v. 35, p. 219-246.

Lide, D.R., 1997: Abundance of elements in the earth's crust and sea, in CRC handbook of physics and chemistry, 78th edition: Boca Raton, Florida, CRC Press, p. 14.

Long, K.R., Van Gosen, B.S., Foley, N.K., and Cordier, Daniel, 2010, The principal rare earth elements deposits of the United States—A summary of domestic deposits and a global perspective: U.S. Geological Survey Scientific Investigations Report 2010–5220, 96 p. Retrieved from: http://pubs.usgs.gov/sir/2010/5220/

MacHattie, T. G., 2011: Nature and setting of late Devonian-early carboniferous rare earth element mineralization in the eastern cobequid highlands, nova scotia. in Mineral Resources Branch, Report of Activities 2010, Nova Scotia Department of Natural Resources, Report ME 2011-1, p. 75-92.

Miller, C. F., Mittlefehldt, D. W., 1982: Depletion of light rare-earth elements in felsic magmas. Geology, v. 10, p. 129-133.

Mitchell, R. H., 1990: A review of the compositional variation of amphiboles in alkaline plutonic complexes. Lithos, v. 26, p. 135-156.

Murphy, J. B., Waldron, J. W. F., Kontak, D. J., Pe-Piper, G., Piper, D. J. W., 2011: Minas Fault Zone: Late Paleozoic history of an intra-continental orogenic transform fault in the Canadian Appalachians. Journal of Structural Geology v. 33, p. 312-328.

Papoutsa, A. 2011: The petrological evolution of the Late Paleozoic A-type granites of the Wentworth plutonic complex of the Cobequid Shear Zone. Unpublished master's thesis, Saint Mary's University, Halifax, Nova Scotia.

Pe-Piper, G., Reynolds, P.H., Nearing, J., Piper, D.J.W. 2004: Early Carboniferous deformation and mineralization in the Cobequid shear zone, Nova Scotia: an 40Ar/39Ar geochronology study. *Can. J. Earth Sci*., v. 41, 1421–1426.

Pe-Piper, G., Piper, D. J. W., 2002: A synopsis of the geology of the Cobequid Highlands, Nova Scotia. Atlantic Geology, v. 38, p. 145-160.

Philpotts, A. R., 1989: Petrography of igneous and metamorphic rocks. Englewood Cliffs, N.J.: Prentice Hall. p. 178.

Salvi, S., Williams-Jones, A. E., 1996: The role of hydrothermal processes in concentrating high-field strength elements in the Strange Lake peralkaline complex, northeastern Canada. Geochimica et Cosmochimica Acta, v. 60(11), p. 1917-1932.

Schmitt, A. K., Trumbull, R. B., Dulski, P., Emmermann, R., 2002: Zr-Nb-REE Mineralization in peralkaline granites from the amis complex, brandberg (Namibia): evidence for mamatic Pre-enrichment from melt inclusions. Economic Geology, v. 97, p. 399-413.

Sun, S. S., McDonough, W. F., 1989: Chemical and isotopic systematics of ocean basalts: implications for mantle composition and processes. London: Geological Society, v. 42, p. 313-345

The Canadian Chamber of Commerce. (2012). Canada's rare earth deposits can offer a substantial competitive advantage. Retrieved from: http://www.chamber.ca/images/uploads/Reports/2012/201204RareEarthElements.pdf

U.S. Congressional Research Service. China's Rare Earth Industry and Export Regime: Economic and Trade Implications for the United States. (R42510; April 30, 2012), by Wayne M. Morrison and Rachel Tang. Retrieved from: http://www.fas.org/sgp/crs/row/R42510.pdf

Williams, H., Hatcher, R. D., 1982: Suspect terranes and accretionary history of the Appalachian orogeny. Geology, v. 10, p. 530-536.

APPENDIX A: FUS-ICP-MS AND FUS-ISE RESULTS

Analyte	Unit	Detection Limit	10TM0024	10TM0026	10TM0036	10TM0049	10TM0052	10TM0056	10TM0057
			granite dyke float	granite dyke	granite dyke	granite dyke float	granite dyke	granite dyke float	granite dyke float
Cl	%	0.01	< 0.01	< 0.01	0.02	0.01	0.04	0.01	0.03
F	%	0.01	0.08	0.19	0.38	1.36	0.23	0.06	0.29
SiO2	%	0.01	74.96	74.14	70.42	64.99	70.12	57.09	66.98
Al2O3	%	0.01	6.96	8.02	6.99	7.30	10.33	13.19	6.78
Fe2O3(T)	%	0.01	7.77	6.81	12.27	10.82	7.51	7.76	12.83
MnO	%	0.001	0.145	0.109	0.144	0.113	0.211	0.139	0.107
MgO	%	0.01	0.1	0.03	0.12	0.7	0.24	1.3	0.6
CaO	%	0.01	0.97	0.89	1.31	4.71	3.84	4.46	1.69
Na2O	%	0.01	1.43	1.66	1.48	2.36	2.15	4.47	0.76
K2O	%	0.01	3.85	4.67	3.58	0.72	2.96	0.07	3.5
TiO2	%	0.001	0.624	0.414	0.433	1.019	0.301	1.074	0.821
P2O5	%	0.01	0.03	0.03	0.05	0.08	< 0.01	0.04	0.09
LOI	%		0.52	0.42	0.74	2.65	1.23	3.18	1.47
Total	%	0.01	97.38	97.19	97.53	95.46	98.9	92.76	95.64
Ba	ppm	3	67	89	72	57	83	57	119
Y	ppm	2	3263	2700	1013	3521	713	6182	4774
Zr	ppm	4	9483	> 10000	7321	> 10000	5293	> 10000	> 10000
Cr	ppm	20	< 20	< 20	< 20	30	< 20	< 20	< 20
Nb	ppm	1	> 1000	> 1000	> 1000	> 1000	967	> 1000	> 1000
La	ppm	0.1	898	567	716	679	260	1030	283
Ce	ppm	0.1	2320	1520	1690	1620	606	2460	961
Pr	ppm	0.05	310	196	211	197	79.2	303	141
Nd	ppm	0.1	1320	807	823	732	325	1100	583
Sm	ppm	0.1	439	290	202	254	96.9	382	257
Eu	ppm	0.05	16.9	11.4	6.81	9.89	3.57	17	12
Gd	ppm	0.1	494	334	170	283	97.1	463	321
Tb	ppm	0.1	97.6	75.9	31.4	79.2	19.6	144	103
Dy	ppm	0.1	621	519	206	624	134	> 1000	884
Ho	ppm	0.1	126	115	43.4	156	28.8	299	226
Er	ppm	0.1	353	346	131	529	90.4	> 1000	799
Tm	ppm	0.05	47.5	49.4	20.1	88.7	14.1	172	133
Yb	ppm	0.1	277	302	130	598	91.5	> 1000	885
Lu	ppm	0.04	37	41.4	19.2	84.4	13.4	159	126
Hf	ppm	0.2	280	469	214	783	175	814	672
Th	ppm	0.1	211	247	215	1430	101	> 2000	1900
U	ppm	0.1	222	176	374	307	95	452	390
Sum REE	ppm		7357	5174	4400	5934	1860	6529	5714

Analyte Symbol	Unit Symbol	Detection Limit	09TM028A	09TM029	09TM117	09TM120	09TM125	09TM126	09TM133	09TM134
			HLBL granite	HLBL granite	HLBL granite	HLBL granite	HLBL granite	HLBL granite	HLBL granite	HLBL granite
F	%	0.01	74	75	75	77	77	77	78	78
SiO2	%	0.01	13.3	12.9	12.8	12.2	11.3	11.5	11.9	11.8
Al2O3	%	0.01	2.7	2.2	2.1	2.2	2.8	2.9	1.9	2.0
Fe2O3(T)	%	0.01	0.1	0.1	0.0	0.0	0.0	0.1	0.0	0.0
MnO	%	0.001	0.1	0.1	0.2	0.1	0.0	0.1	0.1	0.1
MgO	%	0.01	0.5	0.2	0.4	0.3	0.1	0.2	0.3	0.2
CaO	%	0.01	4.0	4.3	3.6	3.4	3.9	3.9	3.5	3.5
Na2O	%	0.01	5.0	4.8	5.5	5.2	4.8	4.9	5.1	5.1
K2O	%	0.01	0.2	0.1	0.2	0.2	0.1	0.2	0.1	0.2
TiO2	%	0.001	0.0	0.0	0.0	0.0	< 0.01	< 0.01	< 0.01	< 0.01
P2O5	%	0.01	0.6	0.3	0.5	0.5	0.2	0.2	0.2	0.2
LOI	%	0.01	0.6	0.3	0.5	0.5	0.2	0.2	0.2	0.2
Total	%	0.01	100.5	99.9	100.6	100.9	100.7	100.7	100.7	100.8
Ba	ppm	3	26	20	21	27	6	11	14	13
Y	ppm	2	502	446	229	310	718	785	341	429
Zr	ppm	4	< 20	80	< 20	< 20	< 20	< 20	60	70
Cr	ppm	20	1	< 1	1	1	< 1	1	< 1	< 1
Nb	ppm	1	2	> 100	4	3	2	< 2	45	7
La	ppm	0.1	106	60.1	132	94.5	132	111	105	139
Ce	ppm	0.1	11.7	5.72	16.2	8.35	15.4	14.9	10.3	18.2
Pr	ppm	0.05	40.5	19.6	54.6	29.6	55.3	54.9	39.3	70.5
Nd	ppm	0.1	9.3	5.1	10.9	6.9	13.6	15.4	10.1	16.8
Sm	ppm	0.1	0.47	0.26	0.36	0.47	0.53	0.76	0.42	0.74
Eu	ppm	0.05	8.7	5	9.3	6.1	12.9	15.4	9.6	14.4
Gd	ppm	0.1	1.8	1.2	1.8	1.3	2.7	3.6	2	2.7
Tb	ppm	0.1	11.4	8	10.9	8.5	17.3	23.7	13	16.6
Dy	ppm	0.1	2.3	1.7	2.2	1.8	3.5	5	2.6	3.2
Ho	ppm	0.1	7.3	5.5	6.7	5.7	11.2	15.1	8	9.6
Er	ppm	0.1	1.2	0.99	1.14	0.99	1.96	2.43	1.32	1.58
Tm	ppm	0.05	8	6.9	7.6	6.9	14.2	17.2	9	10.7
Yb	ppm	0.1	1.19	1.07	1.16	1.07	2.36	2.75	1.4	1.64
Lu	ppm	0.04	16.3	15.7	8.7	11.6	24.8	26.9	13.6	16
Hf	ppm	0.2	5.8	6	3.8	5	8	9.8	4.8	4.8
Th	ppm	0.1	5.9	6	7.8	7	8.1	9.1	5.2	5.1
U	ppm	0.1	210	121	255	172	283	282	212	306
Sum REE			0	280	53	49	943	530	247	365

APPENDIX B: EMP RESULTS AND BSE IMAGES

	10TM0215_1	10TM0215_2	10TM0215_3	10TM0215_4	10TM0215_5	10TM0215_6	10TM0041_1	10TM0041_2	10TM0041_3
SiO2	51.041	51.029	50.582	50.750	50.707	50.186	50.785	50.038	51.137
TiO2	1.372	0.935	1.371	1.417	1.375	1.462	1.025	1.297	1.390
Al2O3	0.318	1.296	0.667	0.642	0.614	0.726	0.635	1.315	0.465
FeO	30.349	31.416	31.853	31.621	32.320	32.545	31.909	32.266	31.358
MnO	0.941	0.608	0.686	0.694	0.677	0.677	0.506	0.524	0.728
MgO	0.363	1.065	0.228	0.023	0.281	0.111	0.500	0.238	0.028
CaO	0.272	1.236	0.604	0.319	0.654	0.603	0.105	0.379	0.202
Na2O	8.908	7.494	9.391	9.435	8.992	8.244	8.392	8.931	9.095
K2O	1.955	0.906	1.208	1.345	1.266	1.262	2.032	1.370	1.578
BaO	0.114	0.149	0.169	0.134	0.139	0.174	0.179	0.136	0.139
F	1.367	1.012	1.442	1.555	1.440	1.206	1.160	1.138	1.350
Cr2O3	0.124	0.174	0.164	0.140	0.169	0.163	0.147	0.171	0.122
Si	8.034	8.008	7.908	7.932	7.911	7.953	8.035	7.898	8.032
Ti	0.162	0.110	0.161	0.167	0.161	0.174	0.122	0.154	0.164
Al	0.059	0.240	0.123	0.118	0.113	0.136	0.118	0.245	0.086
Fe	3.995	4.123	4.165	4.133	4.217	4.313	4.222	4.259	4.119
Mn	0.125	0.081	0.091	0.092	0.089	0.091	0.068	0.070	0.097
Mg	0.085	0.249	0.053	0.005	0.065	0.026	0.118	0.056	0.007
Ca	0.046	0.208	0.101	0.053	0.109	0.102	0.018	0.064	0.034
Na2	2.719	2.280	2.847	2.859	2.720	2.533	2.574	2.733	2.770
K2	0.196	0.091	0.120	0.134	0.126	0.128	0.205	0.138	0.158
Ba	0.007	0.009	0.010	0.008	0.008	0.011	0.011	0.008	0.009
F	0.681	0.502	0.713	0.769	0.711	0.604	0.580	0.568	0.671
Cr	0.015	0.022	0.020	0.017	0.021	0.020	0.018	0.021	0.015

	10TM0041_4	10TM0041_5	10TM0041_6	10TM0041_7	10TM0209_1	10TM0209_2	10TM0209_3	10TM0209_4	10TM0209_5
SiO2	51.316	50.573	48.121	49.176	48.400	50.631	48.188	52.276	50.758
TiO2	1.121	1.078	1.144	1.244	1.381	0.878	1.409	0.739	1.068
Al2O3	0.706	0.933	1.624	1.710	2.413	1.269	2.083	0.445	1.079
FeO	32.783	32.816	29.898	30.278	30.404	32.683	31.865	31.506	31.945
MnO	0.592	0.498	0.468	0.468	0.640	0.945	0.685	1.013	0.626
MgO	0.111	0.060	1.425	1.390	1.467	0.665	1.185	0.805	0.417
CaO	0.128	0.472	1.951	1.234	0.885	0.530	1.086	0.540	0.891
Na2O	8.107	8.326	8.491	8.468	8.294	7.260	8.119	7.048	7.774
K2O	1.609	1.459	1.362	1.489	1.114	0.864	1.138	1.364	1.308
BaO	0.151	0.000	0.000	0.000	0.000	0.000	0.000	0.000	0.000
F	0.785	0.828	2.060	1.790	1.461	0.569	1.453	0.722	1.155
Cr2O3	0.172	0.000	0.008	0.000	0.001	0.015	0.002	0.010	0.000
Si	8.128	8.050	7.577	7.685	7.645	8.092	7.616	8.268	8.003
Ti	0.134	0.129	0.136	0.146	0.164	0.106	0.168	0.088	0.127
Al	0.132	0.175	0.301	0.315	0.449	0.239	0.388	0.083	0.201
Fe	4.342	4.368	3.937	3.957	4.016	4.369	4.212	4.167	4.212
Mn	0.079	0.067	0.062	0.062	0.086	0.128	0.092	0.136	0.084
Mg	0.026	0.014	0.335	0.324	0.345	0.158	0.279	0.190	0.098
Ca	0.022	0.080	0.329	0.207	0.150	0.091	0.184	0.092	0.151
Na2	2.490	2.569	2.592	2.566	2.540	2.250	2.488	2.161	2.376
K2	0.163	0.148	0.137	0.148	0.112	0.088	0.115	0.138	0.132
Ba	0.009	0.000	0.000	0.000	0.000	0.000	0.000	0.000	0.000
F	0.393	0.417	1.026	0.885	0.730	0.288	0.726	0.361	0.576
Cr	0.022	0.000	0.001	0.000	0.000	0.002	0.000	0.001	0.000

	10TM0209_6	10TM0209_7	10TM0209_8	10TM0209_9	10TM0064_1	10TM0064_2	10TM0064_3	10TM0064_4	10TM0064_5
SiO2	50.915	50.697	51.610	50.220	51.386	51.301	50.103	51.191	51.247
TiO2	1.057	1.018	0.723	1.037	1.386	1.304	0.909	0.537	0.981
Al2O3	0.832	0.857	0.819	1.522	0.280	0.294	0.740	0.214	0.525
FeO	32.799	32.558	32.822	30.512	31.785	31.478	32.614	32.015	31.304
MnO	0.630	0.689	0.953	0.744	0.564	0.608	0.550	0.614	0.646
MgO	0.064	0.055	0.457	1.285	0.029	0.037	0.000	0.060	0.090
CaO	0.656	0.565	1.077	0.543	0.143	0.124	0.296	0.090	0.206
Na2O	8.065	8.750	7.903	8.374	8.393	9.161	9.685	9.174	8.345
K2O	1.274	1.322	0.912	1.227	1.904	1.919	1.244	2.180	1.773
BaO	0.000	0.000	0.000	0.000	0.000	0.000	0.000	0.000	0.000
F	1.271	1.332	1.045	1.366	1.135	1.429	1.454	1.481	0.977
Cr2O3	0.023	0.016	0.018	0.024	0.000	0.020	0.007	0.027	0.027
Si	8.004	7.960	8.053	7.881	8.120	8.041	7.908	8.063	8.169
Ti	0.125	0.120	0.085	0.122	0.165	0.154	0.108	0.064	0.118
Al	0.154	0.159	0.151	0.282	0.052	0.054	0.138	0.040	0.099
Fe	4.312	4.275	4.283	4.005	4.201	4.126	4.305	4.217	4.173
Mn	0.084	0.092	0.126	0.099	0.075	0.081	0.074	0.082	0.087
Mg	0.015	0.013	0.106	0.301	0.007	0.009	0.000	0.014	0.021
Ca	0.110	0.095	0.180	0.091	0.024	0.021	0.050	0.015	0.035
Na2	2.458	2.664	2.391	2.548	2.571	2.784	2.964	2.802	2.579
K2	0.128	0.132	0.091	0.123	0.192	0.192	0.125	0.219	0.180
Ba	0.000	0.000	0.000	0.000	0.000	0.000	0.000	0.000	0.000
F	0.632	0.661	0.516	0.678	0.567	0.708	0.726	0.738	0.493
Cr	0.003	0.002	0.002	0.003	0.000	0.002	0.001	0.003	0.003

	10TM0064_6	10TM0064_7	10TM0064_8	10TM0064_9	10TM0064_10	10TM0064_11	10TM0223_1	10TM0223_2	10TM0223_3
SiO2	50.092	50.584	50.167	51.661	51.743	51.828	48.689	50.276	50.157
TiO2	1.030	0.951	1.060	0.740	0.957	0.456	1.419	1.348	1.347
Al2O3	0.743	0.574	0.937	0.309	0.290	0.215	1.522	0.924	0.715
FeO	32.627	31.612	32.845	31.708	31.972	32.765	32.496	31.871	31.046
MnO	0.616	0.749	0.543	0.609	0.558	0.587	0.737	0.837	0.750
MgO	0.283	0.038	0.000	0.006	0.000	0.075	0.142	0.113	0.128
CaO	0.323	0.208	0.554	0.158	0.101	0.078	1.235	0.542	0.565
Na2O	9.317	9.351	8.808	8.906	8.808	8.311	8.493	7.004	8.969
K2O	1.413	1.422	1.374	2.028	1.811	1.853	1.118	1.376	1.368
BaO	0.000	0.000	0.000	0.015	0.000	0.000	0.040	0.005	0.027
F	1.509	1.584	1.248	1.496	1.124	1.085	1.191	0.700	1.553
Cr2O3	0.038	0.014	0.035	0.003	0.000	0.025	0.057	0.062	0.058
Si	7.873	7.972	7.932	8.091	8.151	8.193	7.762	8.131	7.929
Ti	0.122	0.113	0.126	0.087	0.113	0.054	0.170	0.164	0.160
Al	0.138	0.107	0.175	0.057	0.054	0.040	0.286	0.176	0.133
Fe	4.289	4.166	4.343	4.153	4.212	4.332	4.333	4.311	4.105
Mn	0.082	0.100	0.073	0.081	0.074	0.079	0.100	0.115	0.100
Mg	0.066	0.009	0.000	0.001	0.000	0.018	0.034	0.027	0.030
Ca	0.054	0.035	0.094	0.027	0.017	0.013	0.211	0.094	0.096
Na2	2.839	2.857	2.700	2.704	2.690	2.547	2.625	2.196	2.749
K2	0.142	0.143	0.139	0.203	0.182	0.187	0.114	0.142	0.138
Ba	0.000	0.000	0.000	0.001	0.000	0.000	0.002	0.000	0.002
F	0.750	0.789	0.624	0.741	0.560	0.542	0.601	0.358	0.776
Cr	0.005	0.002	0.004	0.000	0.000	0.003	0.007	0.008	0.007

	10TM0223_4	10TM0223_5	10TM0223_6	10TM0223_7	10TM0223_8	10TM0223_9	10TM0223_10	09TM125_1	09TM125_2
SiO2	50.607	51.825	51.733	50.638	50.380	51.490	50.080	49.711	51.494
TiO2	1.291	0.391	0.385	1.060	0.933	0.589	1.025	1.278	0.807
Al2O3	0.687	0.240	0.254	0.899	1.113	0.938	0.850	1.221	0.573
FeO	31.398	29.411	29.249	33.112	30.233	30.793	33.908	32.276	32.181
MnO	0.675	1.228	1.016	0.988	0.763	0.637	0.678	0.611	0.751
MgO	0.087	0.447	0.427	0.143	1.196	1.193	0.150	0.295	0.151
CaO	0.557	0.054	0.015	1.027	1.080	0.427	0.880	1.443	0.067
Na2O	8.680	7.824	8.911	7.175	8.821	8.603	8.924	8.665	8.290
K2O	1.383	2.257	2.364	1.115	1.306	1.337	1.326	1.357	1.891
BaO	0.096	0.007	0.028	0.087	0.036	0.033	0.072	0.048	0.029
F	1.337	1.723	1.739	0.691	1.813	1.740	1.257	1.530	1.297
Cr2O3	0.062	0.048	0.053	0.071	0.067	0.083	0.076	0.075	0.075
Si	8.000	8.192	8.143	8.077	7.822	7.961	7.846	7.771	8.089
Ti	0.154	0.046	0.046	0.127	0.109	0.069	0.121	0.150	0.095
Al	0.128	0.045	0.047	0.169	0.204	0.171	0.157	0.225	0.106
Fe	4.151	3.888	3.850	4.417	3.926	3.982	4.443	4.220	4.228
Mn	0.090	0.164	0.135	0.133	0.100	0.083	0.090	0.081	0.100
Mg	0.021	0.105	0.100	0.034	0.277	0.275	0.035	0.069	0.035
Ca	0.094	0.009	0.003	0.176	0.180	0.071	0.148	0.242	0.011
Na2	2.660	2.398	2.719	2.219	2.655	2.579	2.711	2.626	2.525
K2	0.139	0.228	0.237	0.113	0.129	0.132	0.133	0.135	0.189
Ba	0.006	0.000	0.002	0.005	0.002	0.002	0.004	0.003	0.002
F	0.668	0.861	0.866	0.349	0.890	0.851	0.623	0.756	0.644
Cr	0.008	0.006	0.007	0.009	0.008	0.010	0.009	0.009	0.009

	09TM125_3	09TM125_4	09TM125_5	10TM0052_1	10TM0052_2	10TM0052_3	10TM0052_4	10TM0052_5	10TM0052_6
SiO2	49.906	48.922	49.916	51.319	51.330	50.485	50.306	51.411	50.697
TiO2	1.015	1.297	1.115	1.176	0.386	1.239	1.175	0.686	1.115
Al2O3	0.970	1.361	1.090	0.800	0.850	1.088	1.178	0.799	0.975
FeO	33.098	32.959	32.921	30.086	33.725	29.829	29.815	28.184	30.530
MnO	0.651	0.912	0.660	1.002	0.998	1.350	1.159	1.176	1.180
MgO	0.028	0.310	0.056	0.096	0.020	0.110	0.113	1.993	0.107
CaO	1.372	2.599	0.913	0.125	0.111	0.372	0.226	2.294	0.189
Na2O	8.056	6.571	8.804	8.587	7.801	8.432	9.044	7.231	8.135
K2O	1.120	1.114	1.266	1.413	0.705	1.405	1.443	0.837	1.451
BaO	0.103	0.014	0.058	0.006	0.085	0.061	0.044	0.048	0.038
F	1.467	1.051	1.409	1.969	0.670	1.832	1.990	1.450	1.191
Cr2O3	0.069	0.078	0.085	0.074	0.079	0.069	0.048	0.056	0.048
Si	7.862	7.803	7.841	7.999	8.192	7.937	7.882	8.021	8.082
Ti	0.120	0.156	0.132	0.138	0.046	0.147	0.139	0.081	0.134
Al	0.180	0.256	0.202	0.147	0.160	0.202	0.218	0.147	0.183
Fe	4.361	4.397	4.325	3.922	4.502	3.922	3.907	3.678	4.070
Mn	0.087	0.123	0.088	0.132	0.135	0.180	0.154	0.155	0.159
Mg	0.007	0.074	0.013	0.022	0.005	0.026	0.026	0.464	0.025
Ca	0.232	0.444	0.154	0.021	0.019	0.063	0.038	0.384	0.032
Na2	2.461	2.032	2.682	2.595	2.414	2.570	2.748	2.187	2.514
K2	0.113	0.113	0.127	0.140	0.072	0.141	0.144	0.083	0.148
Ba	0.006	0.001	0.004	0.000	0.005	0.004	0.003	0.003	0.002
F	0.731	0.530	0.700	0.971	0.338	0.911	0.986	0.716	0.600
Cr	0.009	0.010	0.011	0.009	0.010	0.009	0.006	0.007	0.006

	10TM0052_7	10TM0052_8	09TM120_1	09TM120_2	09TM120_3	09TM120_4	09TM120_5	09TM029_1	09TM029_2
SiO2	51.285	51.212	42.595	42.297	42.275	43.051	42.180	46.031	44.398
TiO2	0.971	0.903	1.064	1.306	1.276	1.390	0.990	0.394	0.998
Al2O3	0.731	0.857	7.626	7.593	7.592	7.129	7.664	2.860	4.066
FeO	30.238	30.553	28.334	28.161	28.097	27.846	28.244	31.682	31.032
MnO	1.084	1.076	0.929	0.853	0.893	0.779	0.882	0.940	0.776
MgO	0.106	0.546	4.021	4.017	3.903	4.151	4.248	3.126	2.966
CaO	0.165	0.760	10.355	10.596	10.704	10.660	10.367	8.882	9.340
Na2O	8.924	8.021	2.446	2.369	2.404	2.313	2.431	1.953	2.295
K2O	1.392	1.309	1.190	1.203	1.219	1.045	1.139	0.842	0.929
BaO	0.068	0.053	0.083	0.022	0.060	0.000	0.000	0.000	0.000
F	1.810	1.486	1.023	0.881	0.845	0.766	1.013	0.774	0.611
Cr2O3	0.055	0.066	0.114	0.083	0.091	0.000	0.002	0.121	0.107
Si	8.016	8.028	6.609	6.597	6.604	6.705	6.577	7.349	7.127
Ti	0.114	0.106	0.124	0.153	0.150	0.163	0.116	0.047	0.121
Al	0.135	0.158	1.394	1.396	1.398	1.308	1.409	0.538	0.769
Fe	3.953	4.006	3.676	3.673	3.671	3.627	3.683	4.230	4.166
Mn	0.144	0.143	0.122	0.113	0.118	0.103	0.116	0.127	0.106
Mg	0.025	0.128	0.930	0.934	0.909	0.964	0.988	0.744	0.710
Ca	0.028	0.128	1.721	1.771	1.792	1.779	1.732	1.519	1.607
Na2	2.704	2.438	0.736	0.716	0.728	0.698	0.735	0.605	0.714
K2	0.139	0.131	0.118	0.120	0.121	0.104	0.113	0.086	0.095
Ba	0.004	0.003	0.005	0.001	0.004	0.000	0.000	0.000	0.000
F	0.895	0.737	0.502	0.435	0.417	0.377	0.500	0.391	0.310
Cr	0.007	0.008	0.014	0.010	0.011	0.000	0.000	0.015	0.014

	09TM029_3	09TM029_4	09TM029_5	09TM029_6	09TM029_7	09TM029_8	09TM029_9	09TM029_10	09TM029_11
SiO2	43.622	44.765	44.864	43.300	43.050	43.106	43.341	42.853	43.596
TiO2	0.879	0.594	0.629	1.375	1.343	1.264	1.162	1.081	1.198
Al2O3	4.134	3.735	4.031	4.860	5.264	4.987	5.335	5.441	4.896
FeO	31.557	32.037	31.273	31.217	31.606	31.445	31.007	31.646	32.153
MnO	0.817	0.912	0.881	0.704	0.673	0.718	0.634	0.725	0.896
MgO	2.625	2.757	2.760	2.161	2.048	2.228	2.567	2.211	1.922
CaO	9.166	8.907	9.316	9.979	10.088	10.183	10.065	10.039	9.728
Na2O	2.732	2.378	2.543	2.736	2.781	2.689	2.844	2.665	2.286
K2O	0.778	0.789	0.817	0.929	0.977	0.962	1.008	1.043	1.006
BaO	0.000	0.000	0.000	0.016	0.007	0.039	0.000	0.000	0.000
F	0.660	0.585	0.491	0.599	0.584	0.509	0.604	0.624	0.565
Cr2O3	0.106	0.105	0.106	0.108	0.102	0.104	0.099	0.109	0.115
Si	7.069	7.205	7.199	6.963	6.902	6.937	6.910	6.878	7.001
Ti	0.107	0.072	0.076	0.166	0.162	0.153	0.139	0.131	0.145
Al	0.790	0.708	0.762	0.921	0.995	0.946	1.003	1.029	0.927
Fe	4.277	4.312	4.197	4.198	4.238	4.232	4.135	4.248	4.318
Mn	0.112	0.124	0.120	0.096	0.091	0.098	0.086	0.099	0.122
Mg	0.634	0.662	0.660	0.518	0.489	0.535	0.610	0.529	0.460
Ca	1.592	1.536	1.602	1.719	1.733	1.756	1.719	1.726	1.674
Na2	0.858	0.742	0.791	0.853	0.864	0.839	0.879	0.829	0.712
K2	0.080	0.081	0.084	0.095	0.100	0.099	0.103	0.107	0.103
Ba	0.000	0.000	0.000	0.001	0.000	0.002	0.000	0.000	0.000
F	0.338	0.298	0.249	0.305	0.296	0.259	0.305	0.317	0.287
Cr	0.014	0.013	0.013	0.014	0.013	0.013	0.012	0.014	0.015

	09TM029_12	09TM029_13	09TM029_14	09TM029_15	09TM029_16	09TM029_17
SiO2	43.944	44.097	46.355	46.386	46.503	45.835
TiO2	0.880	1.098	0.607	0.603	0.680	0.936
Al2O3	4.787	4.449	3.226	2.977	2.891	3.550
FeO	31.561	31.896	29.423	31.054	30.906	31.142
MnO	0.770	0.791	0.812	0.819	0.885	0.850
MgO	2.459	2.558	4.755	4.004	4.124	3.617
CaO	9.878	9.715	9.359	9.171	8.590	9.295
Na2O	2.273	2.279	2.311	2.048	2.309	2.150
K2O	1.045	0.909	0.890	0.765	0.735	0.855
BaO	0.000	0.000	0.000	0.000	0.000	0.000
F	0.451	0.538	0.612	0.561	0.656	0.587
Cr2O3	0.086	0.114	0.086	0.082	0.091	0.103
Si	7.055	7.055	7.279	7.325	7.332	7.223
Ti	0.106	0.132	0.072	0.072	0.081	0.111
Al	0.906	0.839	0.597	0.554	0.537	0.659
Fe	4.237	4.267	3.864	4.101	4.075	4.104
Mn	0.105	0.107	0.108	0.110	0.118	0.113
Mg	0.589	0.610	1.113	0.943	0.969	0.850
Ca	1.699	1.665	1.575	1.552	1.451	1.569
Na2	0.707	0.707	0.704	0.627	0.706	0.657
K2	0.107	0.093	0.089	0.077	0.074	0.086
Ba	0.000	0.000	0.000	0.000	0.000	0.000
F	0.229	0.272	0.304	0.280	0.327	0.293
Cr	0.011	0.014	0.011	0.010	0.011	0.013

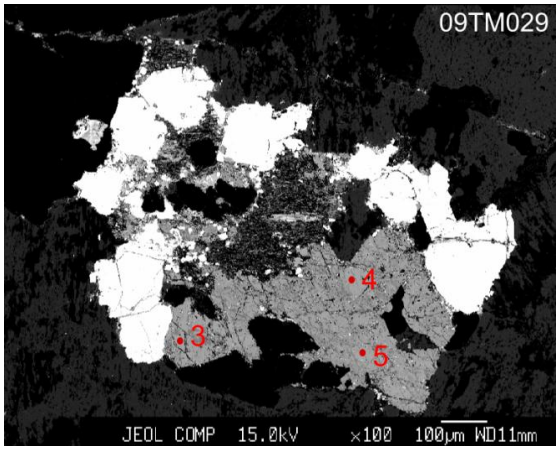
09TM029
3
4
5
JEOL COMP 15.0kV ×100 100µm WD11mm

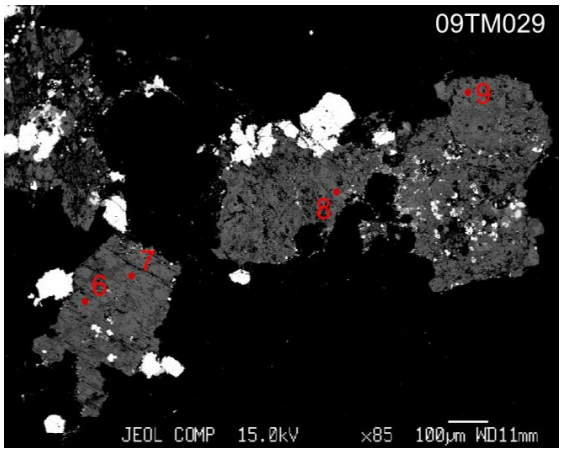
09TM029
6
7
8
9
JEOL COMP 15.0kV ×85 100µm WD11mm

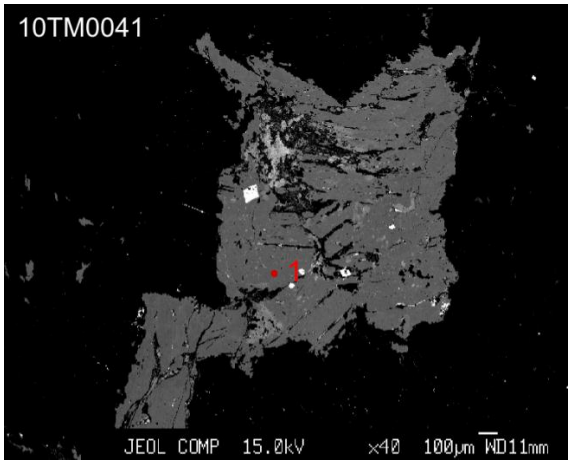
10TM0041
1
JEOL COMP 15.0kV ×40 100µm WD11mm

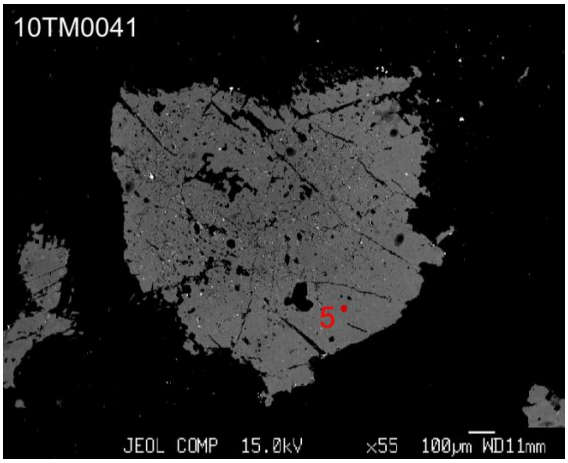
10TM0041
5
JEOL COMP 15.0kV ×55 100µm WD11mm

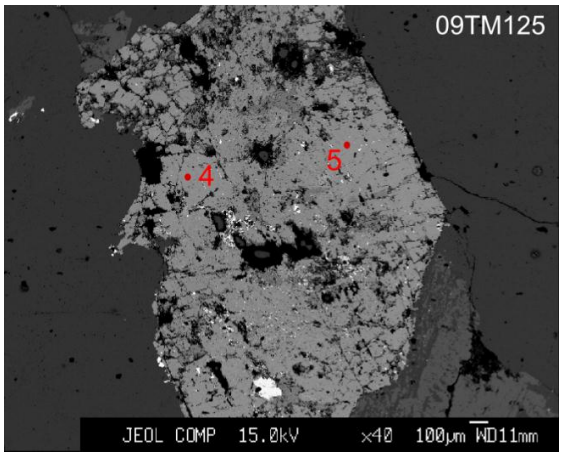
09TM125
4
5
JEOL COMP 15.0kV ×40 100µm WD11mm

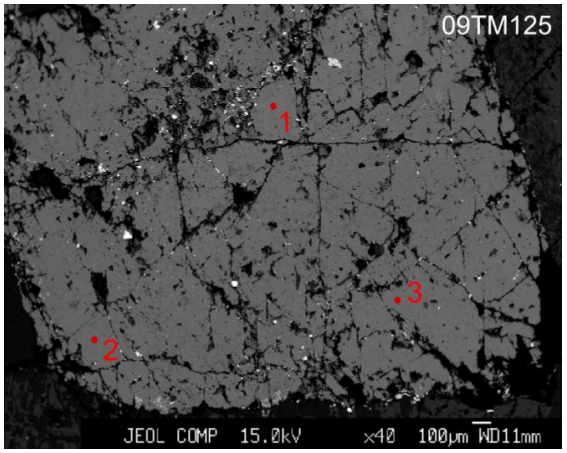
09TM125
1
2
3
JEOL COMP 15.0kV ×40 100µm WD11mm

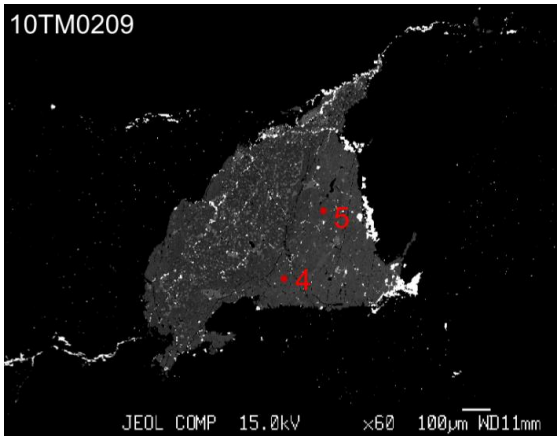
10TM0209
5
4
JEOL COMP 15.0kV ×60 100µm WD11mm

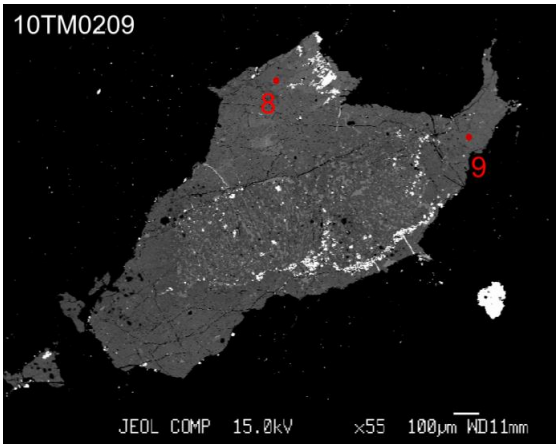
10TM0209
8
9
JEOL COMP 15.0kV ×55 100µm WD11mm

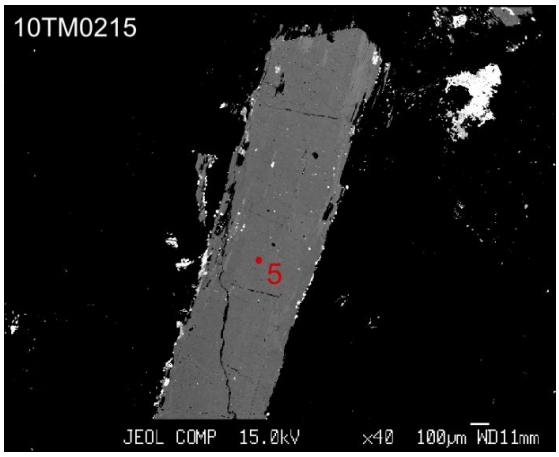
10TM0215
5
JEOL COMP 15.0kV ×40 100µm WD11mm

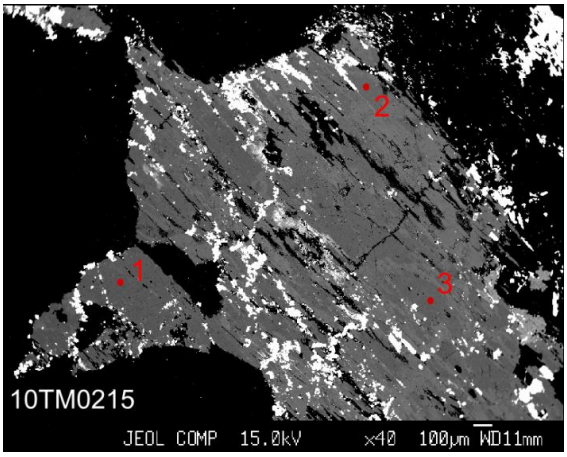
2
1
3
10TM0215
JEOL COMP 15.0kV ×40 100µm WD11mm

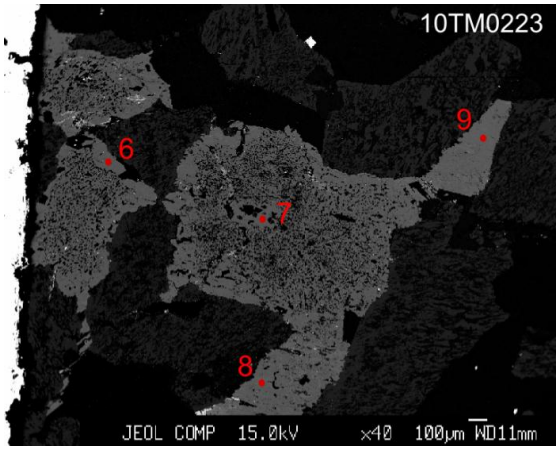
10TM0223
9
6
7
8
JEOL COMP 15.0kV ×40 100µm WD11mm

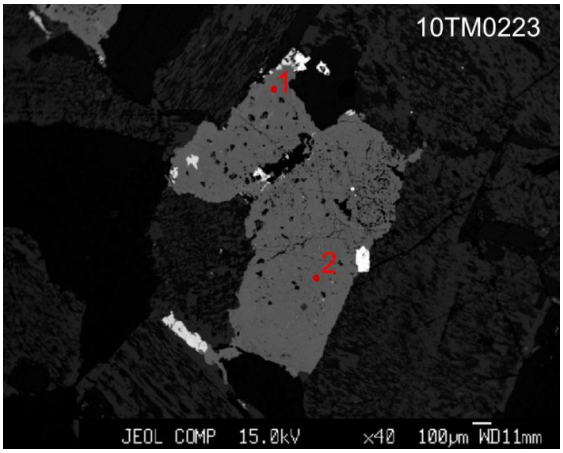
10TM0223
1
2
JEOL COMP 15.0kV ×40 100µm WD11mm

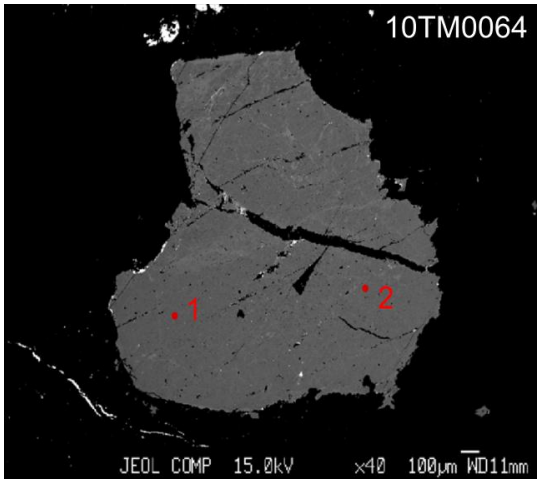
10TM0064
1
2
JEOL COMP 15.0kV ×40 100µm WD11mm

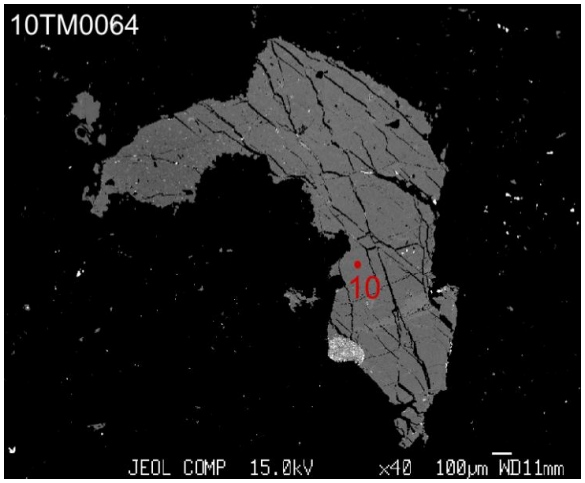
10TM0064
10
JEOL COMP 15.0kV ×40 100µm WD11mm

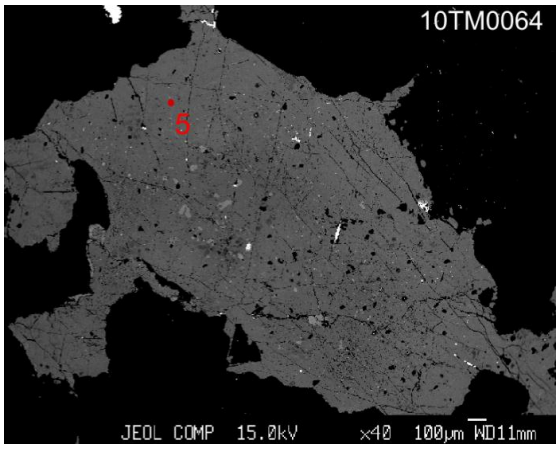
10TM0064
5
JEOL COMP 15.0kV ×40 100µm WD11mm

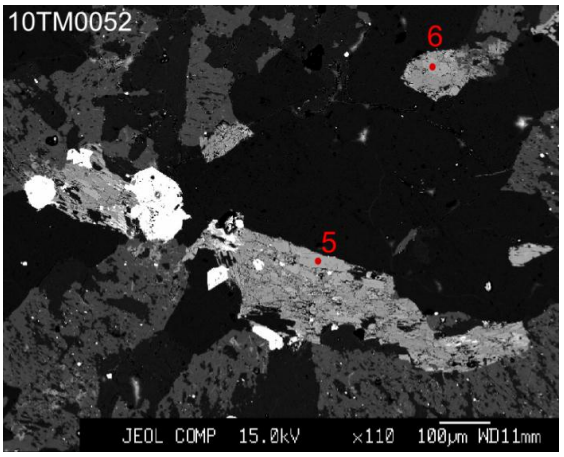
10TM0052
6
5
JEOL COMP 15.0kV ×110 100µm WD11mm

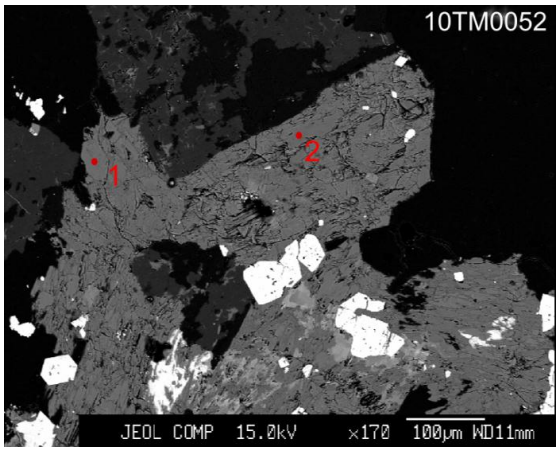
10TM0052
1
2
JEOL COMP 15.0kV ×170 100µm WD11mm

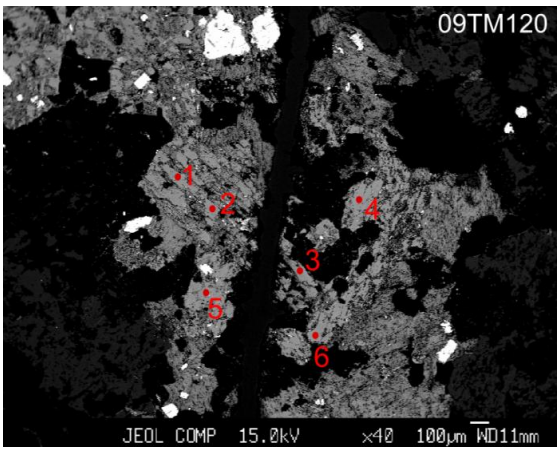
09TM120
1
2
4
3
5
6
JEOL COMP 15.0kV ×40 100µm WD11mm